



Evaluation of carbonyl sulfide biosphere exchange in the Simple Biosphere Model (SiB4)

Linda M.J. Kooijmans¹, Ara Cho¹, Jin Ma², Aleya Kaushik^{3,4}, Katherine D. Haynes⁵, Ian Baker⁵, Ingrid T. Luijkx¹, Mathijs
5 Groenink¹, Wouter Peters^{1,6}, John Miller⁴, Joseph A. Berry⁷, Jerome Ogée⁸, Laura K. Meredith⁹, Wu Sun⁷, Kukka-Maaria
Kohonen¹⁰, Timo Vesala^{10,11,12}, Ivan Mammarella¹⁰, Huilin Chen⁶, Felix M. Spielmann¹³, Georg Wohlfahrt¹³, Max
Berkelhammer¹⁴, Mary E. Whelan¹⁵, Kadmiel Maseyk¹⁶, Ulli Seibt¹⁷, Roisin Commane¹⁸, Richard Wehr^{19,20}, Maarten Krol^{1,2}

¹ Meteorology and Air Quality, Wageningen University and Research, The Netherlands

10 ² Institute for Marine and Atmospheric Research, Utrecht University, The Netherlands

³ Cooperative Institute for Research in Environmental Sciences, University of Colorado Boulder, CO, USA

⁴ NOAA Global Monitoring Laboratory, Boulder, CO, USA

⁵ Department of Atmospheric Science, Colorado State University, USA.

⁶ Centre for Isotope Research, University of Groningen, Groningen, The Netherlands

15 ⁷ Department of Global Ecology, Carnegie Institution for Science, Stanford,
CA, USA

⁸ INRAE, Bordeaux Science Agro, UMR 1391 ISPA, 33140 Villenave d'Ornon, France

⁹ School of Natural Resources and the Environment, University of Arizona, Tucson, AZ 85721, USA

¹⁰ Institute for Atmospheric and Earth System Research/ Physics, Faculty of Science, University of Helsinki, Helsinki, Finland

20 ¹¹ Institute for Atmospheric and Earth System Research/ Forest Sciences, University of Helsinki, Helsinki, Finland

¹² Yugra State University, 628012, Khanty-Mansiysk, Russia

¹³ Department of Ecology, University of Innsbruck, Austria

¹⁴ Department of Earth and Environmental Sciences, University of Illinois at Chicago, Chicago, IL, USA

¹⁵ Department of Environmental Sciences, Rutgers University, New Brunswick, NJ, USA

25 ¹⁶ School of Environment, Earth and Ecosystem Sciences, The Open University, MK 7 6AA Milton Keynes, United Kingdom

¹⁷ Department of Atmospheric & Oceanic Sciences, UCLA, USA

¹⁸ Department of Earth & Environmental Sciences, Lamont Doherty Earth Observatory, Columbia University, Palisades, NY
10964, USA

¹⁹ Department of Ecology and Evolutionary Biology, University of Arizona, USA

30 ²⁰ Currently affiliated at: Center for Atmospheric and Environmental Chemistry, Aerodyne Research, Inc., USA

Correspondence to: Linda Kooijmans (linda.kooijmans@wur.nl)

Abstract. The uptake of carbonyl sulfide (COS) by terrestrial plants is linked to photosynthetic uptake of CO₂ by a shared
diffusion pathway. Applying COS as a photosynthesis tracer in models requires an accurate representation of biosphere COS
fluxes, but these models have not been extensively evaluated against field observations of COS fluxes. In this paper, the COS
35 flux as simulated by the Simple Biosphere Model, version 4 (SiB4) is updated with the latest mechanistic insights and evaluated
with site observations from different biomes: one evergreen needleleaf forest, two deciduous broadleaf forests, three
grasslands, and two crop fields spread over Europe and North America. To account for the effect of atmospheric COS mole



fractions on COS biosphere uptake, we replaced the fixed COS mole fraction originally used in SiB4 with spatially and temporally varying COS mole fraction fields. The lower COS mole fractions in the late growing season reduces COS uptake rates in agreement with observations. We also replaced the empirical soil COS uptake model in SiB4 with a mechanistic model that represents both uptake and production of COS in soils, which improves the match with observations over agricultural fields and fertilized grassland soils. SiB4 was capable of simulating the diurnal and seasonal variation of COS fluxes in the boreal, temperate and Mediterranean region. The daytime vegetation COS flux is on average $8 \pm 27\%$ underestimated, albeit with large variability across sites. On a global scale, our model modifications caused a drop in the COS biosphere sink from 922 Gg S yr⁻¹ in the original SiB4 model to 753 Gg S yr⁻¹ in the updated version. The largest drop in fluxes was driven by lower atmospheric COS mole fractions over regions with high productivity, which highlights the importance of accounting for variations in atmospheric COS mole fractions. The change to a different soil model, on the other hand, had a relatively small effect on the global biosphere COS sink. The small role of the modeled soil component in the COS budget supports the use of COS as a global photosynthesis tracer.

50 **1 Introduction**

Carbonyl sulfide (COS) uptake by the terrestrial biosphere is the main sink of atmospheric COS (Whelan et al., 2018). COS uptake in plants is closely related to photosynthetic CO₂ uptake through its shared uptake pathway through plant stomata and, as a consequence, COS can be used to constrain the carbon and water cycles (Seibt et al., 2010; Stimler et al., 2010; Whelan et al., 2018). Key plant processes such as photosynthesis and transpiration are difficult to observe at scales larger than the leaf level because they are contained within the net CO₂ flux and evapotranspiration and are not separable from other fluxes. Constraints on these fluxes are therefore needed to improve terrestrial biosphere models to better simulate the responses of photosynthesis and stomatal gas exchange to a changing climate. Recently, COS has been shown to be of added value for understanding changes in plant uptake, e.g., the inhibition of photosynthesis during a heat wave (Wohlfahrt et al. 2018), the growth of the terrestrial gross primary production (GPP) during the twentieth century (Campbell et al., 2017), and changes in transpiration (Berkelhammer et al., 2020; Wehr et al., 2017). To further advance COS as a constraint on the carbon and water cycles in models requires an accurate representation and evaluation of COS biosphere fluxes in models.

Biosphere COS exchange has been implemented in land surface models such as the Simple Biosphere Model, version 3 (SiB3; Berry et al. 2013), the Organising Carbon and Hydrology In Dynamic Ecosystems model (ORCHIDEE; Launois et al. 2015a; Maignan et al. 2020), the Lund-Potsdam-Jena model (LPJ) and the Community Land Model (CLM4) (Launois et al. 2015a). Estimates of the global biosphere uptake of COS from these models and other approaches range between 368 and 1845 Gg S yr⁻¹ with a mean of 1084 Gg S yr⁻¹ over 9 different studies as summarized in Table 1 (Kettle et al. 2002; Montzka et al. 2007; Suntharalingam et al. 2008; Berry et al. 2013; Launois et al. 2015a; Kuai et al. 2015; Wang et al. 2016; Maignan et al. 2020; Ma et al. 2021). These estimates were made through different approaches, such as scaling COS vegetation uptake to the net



70 (NPP) or gross primary production (GPP), and more recently also from mechanistic implementations (Table 1). The
mechanistic implementations of COS vegetation uptake in the biosphere models yield a smaller range of 688-775 Gg S yr⁻¹
than when the COS vegetation uptake is scaled to the CO₂ vegetation sink (Table 1). The global soil COS sink estimates range
from 130 to 510 Gg S yr⁻¹, but with most estimates between 130 and 176 Gg S yr⁻¹. However, land surface models have still
not adopted the available mechanistic soil models from either Sun et al. (2015) or Ogée et al. (2016).

75

It was pointed out by Ma et al. (2021) that the temporal and spatial variability of atmospheric COS mole fractions has
considerable influence on the COS biosphere uptake; e.g. a seasonal amplitude of ~100-200 parts per trillion (ppt) around an
average of ~500 ppt affects the fluxes by ~20-40 %. In contrast to CO₂, where a seasonal amplitude of ~6-7 ppm around ~410
ppm affects the fluxes only by ~2 %. Although some of the previous studies considered the variable COS mole fraction already
80 (Berry et al., 2013, Kuai et al., 2015, Wang et al., 2016), it has not yet been adopted as a standard approach (Maignan et al.
2021, Ma et al., 2021).

Inverse modeling studies that account for all known sources and sinks of COS imply a missing source of COS in the tropical
region (Berry et al. 2013; Le Kuai et al. 2015; Ma et al. 2021). Ma et al. (2021) revealed considerable seasonal variations of
85 the missing source. Yet, the exact reason for this missing source has not been resolved. Although the missing source can be
anthropogenic or from the tropical ocean (Launois et al. 2015b; Kuai et al. 2015; Lennartz et al. 2017, 2019), an overestimated
tropical biospheric sink cannot be ruled out. Moreover, Ma et al. (2021) identified a missing sink at the higher latitudes that
required larger uptake in summer. This missing sink could be explained by an underestimated biosphere sink, and would be
equivalent to a 6 % underestimation of the biosphere sink above 30 °N (Ma et al., 2021).

90

A source of uncertainty for COS uptake by land surface models is that simulations have not been extensively compared against
field observations because field measurements of ecosystem and soil fluxes are sparse. Yet, several research groups have
performed field observations of COS ecosystem fluxes in the last decade (Asaf et al. 2013; Maseyk et al. 2014; Commane et
al. 2015; Kooijmans et al. 2017; Wehr et al. 2017; Yang et al. 2018; Spielmann et al. 2019; Berkelhammer et al. 2020; Vesala
95 et al., in prep) with observations covering evergreen needleleaf forests, deciduous broadleaf forests, grasslands, and crop fields.
These experimental efforts now offer the possibility to compare model simulations of COS biosphere exchange against field
observations from different biomes.

In this paper, we take advantage of these field measurements for comparison with the latest version of the SiB model, version
100 4 (SiB4) and to evaluate the calculated global COS biosphere flux. When compared to SiB3 (Berry et al. 2013), SiB4 has
enhanced capabilities to simulate variable carbon pool allocation, prognostic phenology, land cover heterogeneity, and crop
phenology (Haynes et al. 2019a). We evaluate seasonal and diurnal cycles of ecosystem COS fluxes and the representativeness
of nighttime COS uptake, where the latter is important for an accurate COS sink estimate. We furthermore update the SiB4



105 model with knowledge obtained on soil exchange of COS during the last decade by implementing the mechanistic soil model
from Ogée et al. (2016) for COS soil uptake and production rates varying with biome after Meredith et al. (2018, 2019).
Furthermore, we replace the fixed atmospheric COS mole fraction of 500 pmol mol⁻¹ with spatially and temporally varying
COS mole fraction fields obtained from an inversion with the TM5-4DVAR atmospheric transport model (Ma et al., 2021).
We diagnose possible biases from the model-observation comparison and conclude with recommendations for further
improvement of the model.

110

115

120

125

130

135



Table 1. Global vegetation, soil and biosphere COS sink estimates presented in literature and this study (Gg S yr⁻¹)

	Kettle et al. (2002)	Montzka et al. (2007)	Suntharalingam et al. (2008)	Berry et al. (2013)	Kuai et al. (2015)	Wang et al. (2016)	Launois et al. (2015a)	Maignan et al. (2021)	Ma et al. (2021)	This study			
										Original SiB4	Modified SiB4		
Vegetation	238	1115	490	738	775	688	1335 (708 ^c)	1069 (663 ^c)	930 (772 ^c)	756	-	776	664
Method	NPP scaling	NPP scaling	NPP scaling	SiB3	SiB3	SiB3	GPP scaling, ORC	GPP scaling, LPJ	GPP scaling, CLM4	ORC	SiB4	SiB4	SiB4 ^d
Soil	130	127 ^a	130 ^a	355	176	159	513 (283 ^c)	513 (398 ^c)	513 (507 ^c)	-	-	146	89
Method	Soil model ^b	Soil model ^b	Soil model ^b	SiB3 ^c	SiB3 ^c	SiB3 ^c	Scaling to H ₂ deposition			SiB4 ^c	SiB4 ^c	SiB4 ^c	SiB4 ^{d,e,f}
Total biosphere sink	368	1242	620	1093 ^d	951	847	1845	1579	1440	1053 (851 ^e)	922	753	

^a Adopted from Kettle et al. (2002)

^b Following Kesselmeier et al. (1999)

^c Scaled to heterotrophic CO₂ respiration

^d Considering a variable mixing ratio

^e After optimization

^f Following Ogée et al. (2016)



2. Methodology

140 2.1 SiB4 model

The Simple Biosphere Model version 4 (SiB4) is a mechanistic, prognostic land surface model that integrates heterogeneous land cover, environmentally responsive prognostic phenology, dynamic carbon allocation, and cascading carbon pools from live biomass to surface litter to soil organic matter (Haynes et al. 2019a,b). SiB4 predicts vegetation and soil moisture states, land surface energy and water budgets, and the terrestrial carbon cycle. Rather than relying on satellite data as in SiB3, SiB4
145 fully simulates the terrestrial carbon cycle by using the carbon fluxes to determine the above and belowground biomass, which in turn feeds back to impact carbon assimilation and respiration (Haynes et al. 2020). SiB4 predicts plant phenology, divided into different stages, allowing the change of photosynthetic activity over the season through specified maximum RuBisCO velocities in each phenological stage. To classify land surface vegetation, SiB4 uses plant functional types (PFTs), which group plants according to their function and physical, physiological, and phenological characteristics. In addition to nine natural
150 vegetation PFTs, SiB4 includes three specific crops (maize, soybeans, and winter wheat), and two generic crops (C3 and C4) following the crop phenology model developed by Lokupitiya et al. (2009). SiB4 includes land cover heterogeneity by simulating multiple PFTs per grid cell.

2.1.1 COS plant and soil uptake after Berry et al. (2013)

COS plant uptake in the SiB4 model has been described by Berry et al. (2013) and is simulated as a series of conductances (g_t)
155 from the leaf boundary layer to the site of COS hydrolysis in the mesophyll cells. These conductances include the conductance from canopy air to the leaf surface, or leaf boundary layer conductance (g_b), the stomatal conductance (g_s), and the internal conductance (g_{cos}). The latter represents both the diffusion of COS to the mesophyll cells and the efficiency of the leaf mesophyll carbonic anhydrase (CA) to hydrolyze COS. This leads to the following equation for the COS uptake rate by vegetation:

$$F_{cos,veg} = C_a \frac{1}{\frac{1.94}{g_s} + \frac{1.56}{g_b} + \frac{1}{g_{cos}}} = C_a g_t, \quad (1)$$

160 where $F_{cos,veg}$ is the COS vegetation uptake rate ($\text{pmol m}^{-2} \text{s}^{-1}$) and C_a is the COS mole fraction in the canopy air space (pmol mol^{-1}) calculated from the mixed layer COS mole fraction (standard $500 \text{ pmol mol}^{-1}$, but see Sect. 2.1.3.) taking into account uptake of COS by soil and vegetation in the previous timestep. g_s and g_b are the stomatal and boundary layer conductances to water vapor ($\text{mol m}^{-2} \text{s}^{-1}$), respectively, and are scaled with diffusivity ratios to account for the different diffusivity rates of COS and H_2O (Seibt et al., 2010; Stimler et al., 2010). The stomatal conductance g_s is derived following the Ball-Berry
165 photosynthesis-conductance model as modified by Collatz et al. (1992) and g_b follows the formulations described by Sellers et al. (1996). The internal conductance g_{cos} is assumed to scale with maximum carboxylation rate of RuBisCO, V_{max} ($\mu\text{mol m}^{-2} \text{s}^{-1}$) (Berry et al. 2013), inspired by previous findings that both CA activity (Badger and Price, 1994), and mesophyll



conductance (Evans et al., 1994) scale with V_{max} in C3 species. In SiB4, V_{max} is adjusted to canopy temperature (T_{can}) following (Sellers et al., 1992):

$$V_{maxT} = V_{max} 2.1^{0.1(T_{can}-298.0)}, \quad (2)$$

170 g_{cos} is then described as:

$$\begin{cases} g_{cos} = \alpha \cdot V_{COS} \\ V_{COS} = V_{maxT} \cdot F_{LC} \cdot F_{RZ} \cdot \left(\frac{p}{p_{0sfc}}\right) \cdot \frac{T_{can}}{T_0} \end{cases} \quad (3)$$

where F_{LC} is a factor scaling the flux from a single leaf to the canopy that considers the canopy profile of absorbed photosynthetically active radiation (Sellers et al., 1996), F_{RZ} is the rootzone water potential, an empirical scaling factor that reduces the biochemical activity when little soil moisture is available (e.g. during extended periods of drought), p/p_{0sfc} adjust the fluxes for altitude, where p is atmospheric pressure (hPa) and p_{0sfc} the reference surface pressure (1000 hPa), and T_{can}/T_0 scales the flux to a reference temperature at $T_0 = 273.15$ K. A calibration term α was added to scale g_{cos} to COS flux observations of controlled gas exchange measurements (Stimler et al., 2010, 2011), which resulted in $\alpha = 1200$ for C3 and 13000 for C4 species (Berry et al. 2013). These numbers were later updated to $\alpha = 1400$ and 8862 for C3 and C4 species, respectively, after updates were made to the SiB model. Berry et al. (2013) already noted that the α value did not constrain the variability between plant species well, likely due to plant variability in CA activity and/or differences in mesophyll conductance. In Sect. 2.3 we explain how we use field measurements to explore whether we can refine α values for different plant functional types separately and to make it variable over time.

The enzyme CA is expressed in microbial communities in soils as well, leading to COS uptake by soils (e.g. Kesselmeier et al., 1999; Meredith et al. 2019). In SiB4, COS uptake in soils (hereafter called “the Berry soil model”) is coupled to heterotrophic CO_2 respiration under the assumption that in more productive regions there would be more litter and surface soil carbon for respiration, and these richer carbon environments would have more CA as well (Yi et al., 2007). Additionally, COS soil uptake in the model is regulated by diffusion, controlled by soil porosity and the fraction of water filled pore space (Van Diest and Kesselmeier, 2008; Ogée et al., 2016; Sun et al., 2015; Whelan et al., 2016). Initial implementations of soil COS uptake made calculations for the entire soil column, but subsequent model versions considered only uptake in the top 20 cm of the soil (Wang et al. 2016), thereby decreasing global soil uptake estimates from 355 (Berry et al. 2013) to 159 Gg S yr⁻¹ (Wang et al. 2016). In the next section, we describe our update to the SiB4 model based on advances in our knowledge on COS soil exchange obtained during the last decade.



2.1.2 Mechanistic COS soil model after Ogée et al. (2016)

Field and laboratory experiments in the last decade showed that COS is not only taken up by soil but is also produced due to abiotic thermal degradation and photodegradation of soil organic matter and is especially enhanced in agricultural soils (Maseyk et al. 2014; Whelan and Rhew 2015; Meredith et al. 2018; Kaisermann et al. 2018a). Besides COS soil production being enhanced in fertilized soils, COS uptake was shown to be diminished in fertilized soils (Kaisermann et al. 2018b). These effects of nutrient fertilization on soil COS exchange were initially not simulated in the SiB4 model.

New empirical soil models (Whelan et al., 2016) and mechanistic models (Ogée et al., 2016; Sun et al., 2015) were developed during the last decade. The mechanistic models describe the uptake and production pathways together with COS diffusion in a soil column. Ogée et al. (2016) derived a simplified analytical solution assuming a soil column with uniform temperature, soil moisture, and porosity and steady state conditions for comparison against laboratory measurements. The model from Ogée et al. (2016), hereafter called “the Ogée soil model”, was then used by several laboratory studies to study patterns in uptake and production of COS in soils (Meredith et al. 2018; 2019; Kaisermann et al. 2018a,b). Due to these efforts, there are now reaction rate parameter values available for a range of biomes and land use types. Because these reaction rate values were derived by fitting the Ogée soil model on data from mesocosm experiments, they should be used in combination with this model to estimate ecosystem-scale soil COS fluxes. Also, compared to the COS soil model proposed by Sun et al. (2015), the steady state solution of the Ogée soil model is computationally inexpensive and therefore more suitable for implementation in SiB4 for global COS soil flux calculations. In the following paragraphs we describe the implementation of the Ogée soil model in SiB4.

For field conditions (assuming a zero COS vertical gradient at the bottom of the soil layer and steady state) the COS soil flux (mol m⁻² s⁻¹) calculation simplifies to (Ogée et al., 2016):

$$F_{COS,soil} = \sqrt{kB\theta D} \cdot \left(C_a - \frac{z_1^2 P}{D} \left(1 - \exp\left(\frac{z_p}{z_1}\right) \right) \right), \quad (4)$$

where k is the CA reaction rate (s⁻¹), B (m³ water m⁻³ air) the solubility of COS in water that relates to Henry’s law constant and depends on temperature, θ the soil water content (m³ m⁻³), D the soil COS diffusivity (m³ air m⁻¹ soil s⁻¹), C_a the COS mole fraction at the soil-air interface, $z_1^2 = D/(kB\theta)$, and P the COS production rate (mol m⁻³ s⁻¹) uniform over depth z_p (here assumed to be 1.0 m). For details of the model calculations we refer to Ogée et al. (2016), here we provide the information specific for the implementation in SiB4. We assume C_a to be identical to the COS mole fraction in the canopy air space. While implementing and testing the model we recognized the strong dependence of the soil fluxes on soil porosity, choice of tortuosity functions, and the SiB4 soil layer selected for temperature and soil moisture. For the calculation of D we used the SiB4 soil porosity (m³ m⁻³; calculated from sand fractions following Lawrence and Slater (2008)) that accounts for the volume of ice in the soil. The simulated soil water content and soil temperature are taken from the top 5 cm soil layer, where most of the COS



uptake takes place. D also depends on tortuosity functions that describe the tortuous movement through the air- or water-filled
225 pore space. Several tortuosity functions are described in the literature and also Ogée et al. (2016) acknowledged that the
response of the soil COS fluxes to soil moisture varied with the chosen tortuosity functions. We chose the tortuosity functions
of Deepagoda et al. (2011) for air and Millington and Quirk (1961) for water, as these functions do not require a pore-size
distribution parameter, which facilitates its implementation in SiB4.

230 COS is taken up in soils through hydrolysis in soil water, where the main consumption is enzymatic, and thus depending on
soil CA enzyme activity. Here, and following other studies (i.e. Ogée et al. 2016, Meredith et al. 2019), we expressed the CA
reaction rate k relative to the uncatalyzed reaction rate (k_{uncat}) at a reference temperature (T_{ref}) and pH:

$$k = f_{CA} k_{uncat} \frac{x_{CA}(T)}{x_{CA}(T_{ref})}, \quad (5)$$

where f_{CA} is the CA enhancement factor, k_{uncat} varies with soil pH according to Elliott et al. (1989) and $x_{CA}(T)$ and $x_{CA}(T_{ref})$ are
temperature response functions (Ogée et al., 2016).

235

Meredith et al. (2019) collected soils from 20 sites from different biomes. Using controlled laboratory measurements, they
derived k_{cat} , k_{uncat} and f_{CA} from a range of biomes and land use types. In SiB4 we used the biome averaged f_{CA} from Meredith
et al. (2019) for calculation of COS soil uptake across different PFTs (Table 2).

240 The COS production was defined by Ogée et al. (2016) as a temperature response function modulated by the soil redox
potential. Meredith et al. (2018) also measured COS production at a temperature range between 10 and 40 °C for a range of
biomes. Measurements were then fitted to an exponential model:

$$P = a \exp(bT_{soil}). \quad (6)$$

We used this exponential temperature model and the biome averaged a and b (Table 2) in our calculation of P in SiB4. We
assume here that the controlled laboratory measurements by Meredith et al. (2018; 2019) can be used to estimate soil fluxes
245 under field conditions.

250



Table 2. Biome-averaged uptake and production parameters after Meredith et al. (2018; 2019).

	Production parameters ^a		Uptake parameter ^b
	$a \pm \text{std}$ ($\text{pmol m}^{-3} \text{s}^{-1}$)	$b \pm \text{std}$ ($1/^\circ\text{C}$)	f_{CA}
Grass	2.20 ± 0.5	0.096 ± 0.005	45000 ^c
Evergreen forest	4.86 ± 2.7	0.101 ± 0.015	32000 ^d
Deciduous forest	4.94 ± 0.7	0.107 ± 0.002	32000 ^d
Agriculture	9.59 ± 7.3	0.104 ± 0.004	6500
Desert/Bare soil	5.60 ± 5.1	0.050 ± 0.010	13000 ^e

^aBased on Meredith et al. (2018)

255 ^bBased on Meredith et al. (2019)

^cMeasurements represent tropical grassland

^dMeasurements represent temperate coniferous and temperate broadleaf forests

^eMeasurements represent desert soil

2.1.3 Variable atmospheric COS mole fractions

260 The atmospheric COS mole fraction in the planetary boundary layer affects both the COS vegetation and soil flux calculations (Eq. (1) and (4)). In SiB4 a standard constant “place-holder” COS mole fraction of $500 \text{ pmol mol}^{-1}$ is used. Ma et al. (2021) estimated that the global biosphere sink would decrease from $1053 \text{ Gg S yr}^{-1}$ to 851 Gg S yr^{-1} if the fixed COS mole fraction were replaced with monthly mean fields that account for the drawdown of COS near the surface in the peak growing season. We thus changed the prescribed COS mole fraction from a fixed value to one varying in space and time, including seasonal and diurnal variability. To this end we used the surface COS mole fraction fields at a global resolution of $4^\circ \times 6^\circ$ (latitude \times longitude) at 3-hourly time steps as retrieved from an atmospheric transport inversion performed with TM5-4DVAR by Ma et al. (2021) using the chemistry transport model TM5 in which COS exchange was recently implemented. Atmospheric measurements of COS mole fractions at 14 sites from the National Oceanic and Atmospheric Administration (NOAA) flask network (Montzka et al., 2007) were used to optimize the sources and sinks of COS. Here, we used global 2D surface layer fields of COS mole fractions that were determined for the period 2016-2018 and repeated the average over those years as input to the SiB4 mixed layer COS mole fraction for each year in the simulation (see global maps of monthly mean surface COS mole fractions in supplementary figure S13 of Ma et al. (2021)). The changing (e.g. lower) COS mole fractions would lead to lower COS uptake rates, but would in turn also lead to a smaller drop in COS mole fractions, this feedback is currently not accounted for.

275 2.1.4 Simulations

We used meteorological data from the Modern-Era Retrospective Analysis for Research and Applications, version 2 (MERRA), which are available from 1980 onwards (Gelaro et al., 2017) as meteorological forcing to SiB4. To ensure realistic



rainfall, the convective and large-scale precipitation values were scaled such that the monthly total rainfall matches with the monthly precipitation in the Global Precipitation Climatology Project, Version 1.2 product (Huffman et al. 2001; Baker et al. 2010; Haynes et al. 2019a,b). Up to 10 PFTs per grid cell (at $0.5^\circ \times 0.5^\circ$ resolution) are prescribed following PFT maps based on MODIS data (Lawrence and Chase, 2007). The soil characteristics such as sand fraction (used for the calculation of soil porosity) are provided by the International Geosphere-Biosphere Programme (IGBP) Global Soil Data Task Group (2000).

We run SiB4 from 2000 to 2020, the simulations were preceded by a spinup iterating five times over the years 2000-2020 to initialize the carbon pools to reach steady state. CO_2 mole fractions were held constant at $370 \mu\text{mol mol}^{-1}$ during spinup and simulations. We performed two sets of four simulations (global and site level) with the same driver data and settings, but with a different temporal resolution of the output: 1. For global simulations, we used monthly averaged output. Moreover, SiB4 simulates multiple PFTs per grid cell. These were averaged, weighted by the fraction of land area occupied by each PFT; 2. To compare SiB4 with site observations (listed in Table 3), we run the SiB4 model with 3-hourly output for only the grid cells (at $0.5^\circ \times 0.5^\circ$ resolution) in which the sites are located. For comparison with observations we selected the PFT that best represents the measurement site.

We run SiB4 with four different configurations:

- 1) the original SiB4 model containing the standard COS mole fraction of $500 \text{ pmol mol}^{-1}$ and the Berry soil model (SiB4_500_Berry);
- 2) the Ogée soil model and the standard COS mole fraction of $500 \text{ pmol mol}^{-1}$ (SiB4_500_Ogee);
- 3) the Berry soil model and variable COS mole fractions (SiB4_var_Berry), and
- 4) the Ogée soil model and variable COS mole fractions (SiB4_var_Ogee).

2.2 Field observations

We use existing field observations for comparison with the SiB4 model simulations. Several studies have collected field data in the last two decades and we used those sites where continuous hourly measurements of ecosystem COS fluxes are available for at least a month. The site locations, some of their characteristics, and basic information on the observations are summarized in Table 3. The locations of the sites are indicated in Fig. 1. The measurements represent evergreen needleleaf forest (ENF), deciduous broadleaf forest (DBF), maize (MAI), winter wheat (WWT), and C3 grasslands (C3-GRA), more specifically alpine grassland, prairie grassland, and savannah grassland.

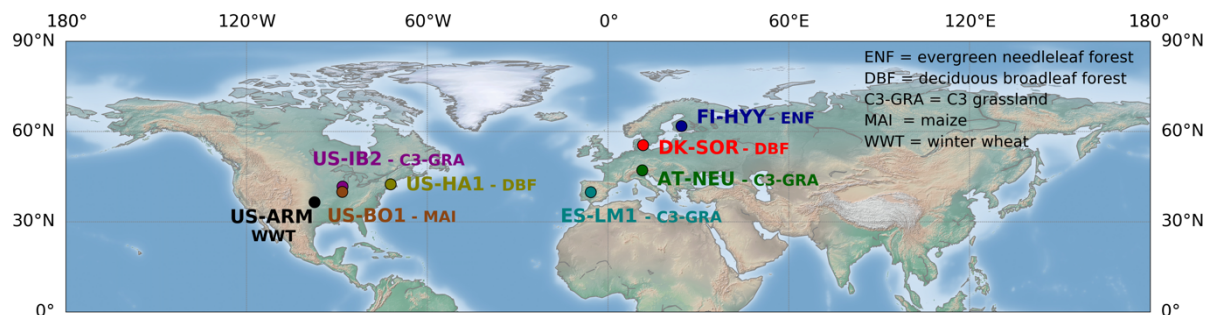


Figure 1. Location of measurement sites and information on the PFT they represent.

310 All COS observations were made at FLUXNET, ICOS or AmeriFlux sites with the benefit that additional long-term
measurements of CO₂ and water exchange (Pastorello et al., 2020) are often available (see Table S1 for an overview), allowing
the evaluation of the SiB4 phenology when COS flux observations do not extend to a full growing season. Most of the
ecosystem observations were made using the eddy-covariance (EC) technique. Kohonen et al. (2020) summarized the different
EC processing steps used by the different studies. Only at US-IB2, US-BO1, and for a part of the dataset at US-HA1 (in 2011),
315 the ecosystem fluxes are derived by COS concentration gradients using the flux-profile (FP) technique (Berkelhammer et al.,
2020; Commane et al., 2015). Ecosystem fluxes are corrected for storage of COS in the canopy airspace using collocated
canopy COS profile measurements when available (FI-HYY and US-HA1).

Most of the selected sites have *in situ* COS soil flux observations available for at least a part of the total measurement period
320 so that the COS uptake by vegetation can be derived from observed ecosystem fluxes. Measurements were collected using soil
chambers, except at US-HA1, where atmospheric profile measurements near the surface were used to calculate the soil fluxes
in 2012 and 2013.

Measurement datasets also include COS mole fractions above the canopy (except for US-ARM). These measurements have
325 been calibrated against the NOAA-2004 COS calibration scale. Only at US-HA1 the COS mole fractions are not calibrated
(Commane et al., 2015), but validated against COS flask measurements at the station, which are part of the NOAA flask
measurement network (Montzka et al., 2007).

For further details about the site characteristics and measurement and processing procedures we refer to the original data
330 publications as reported in Table 3 and Table S1.

For evaluation of the model against observations we calculate the mean bias error (MBE; pmol m⁻² s⁻¹) and root mean square
error (RMSE; pmol m⁻² s⁻¹) for monthly, daytime, and nighttime average fluxes.



335 **Table 3.** Site and measurement information of field observations that are used for comparison with the SiB4 model. Sites are shown from high to low latitude. PFTs covered by the sites are evergreen needleleaf forest (ENF), deciduous broadleaf forest (DBF), C3 grassland (C3-GRA), maize (MAI), and winter wheat (WWT). The ecosystem and soil flux measurement techniques are indicated as eddy-covariance (EC), flux-profile (FP), chamber measurements, or are not available (NA). Mean annual temperature and mean annual precipitation are shown in Table S1.

	Lat (°N), Lon (°E)	SiB4 PFT	Year	Months	Soil flux	Ecosystem flux	Reference
Hyytiälä, Finland (FI- HYY)	61.8, 24.3	ENF	'13 - '17	Jan- Nov	Chamber	EC	Kooijmans et al. 2017; 2019; Sun et al. 2018; Vesala et al. in prep.
Sorø, Denmark (DK-SOR)	55.5, 11.6	DBF	'16	Jun	Chamber	EC	Spielmann et al. 2019
Neustift, Austria (AT-NEU)	47.1, 11.3	C3-GRA (alpine grassland)	'15	Jun- Aug	Chamber	EC	Spielmann et al. 2019; 2020
Harvard Forest, US (US-HA1)	42.5, -72.2	DBF (mixed forest dominated by DBF)	'11 - '13	Apr- Oct	FP ('12- '13)	FP ('11) + EC ('12-'13)	Commane et al. 2015; Wehr et al. 2017
Fermilab, US (US-IB2)	41.8, -88.2	C3-GRA (prairie grassland)	'16 - '17	Apr- Oct	NA	FP	Berkelhammer et al. 2020
Bondville, US (US-BO1)	40.0, -88.3	MAI	'15	Jul/Sep	NA	FP	Berkelhammer et al. 2020
Majadas, Spain (ES-LM1)	39.9, -5.8	C3-GRA (savannah grassland)	'16	May	Chamber	EC	Spielmann et al. 2019
ARM Southern Great Plains, US (US-ARM)	36.6, -97.5	WWT	'12	Apr- May	Chamber	EC	Maseyk et al. 2014

2.3. Calibration factor α

340 Berry et al. (2013) used the calibration factor α to scale g_{cos} to match the simulated COS vegetation flux with laboratory
 measurements. They noted that the α value did not constrain the variability between plant species well, likely due to plant
 variability in CA activity and/or mesophyll conductance. Here, we derived α_{obs} from COS field measurements. This analysis
 is meant to explore its variability over time and the necessity to define α values specific for different PFTs. We did not retain
 α_{obs} for global simulations.

345

We derived g_t from measurements of canopy vegetation fluxes ($F_{COS,veg}$ = ecosystem – soil fluxes) and simulated COS mole
 fractions in the canopy airspace C_a :



$$g_{t,obs} = \frac{F_{COS,veg}}{C_a} \quad (9)$$

Then, rewriting Eq. (1) and (3) and adopting g_s , g_b and g_{cos} from SiB4 site simulations we calculated α_{obs} as:

$$\alpha_{obs} = \frac{-1}{\frac{V_{cos}}{g_{t,obs}} \left(g_{t,obs} \frac{1.94}{g_s} + g_{t,obs} \frac{1.56}{g_b} - 1 \right)} \quad (10)$$

α_{obs} was calculated for daytime hours (10 – 15 hr local time) in periods with photosynthetically active vegetation, which
350 excludes data points of FI-HYY when plants are dormant in winter (November to April), and after the simulation of harvest at
US-ARM. Raw α_{obs} data points were considered an outlier when their value extends 1.5 times the 25-75 percentile range
outside the quartiles and were removed from the analysis.

This analysis requires that field measurements of ecosystem and soil fluxes are available. Under the assumption that both V_{max}
(and thus photosynthesis) and the soil flux are accurately simulated, the application of α_{obs} would result in simulated COS
355 vegetation fluxes that match with observations.

3. Results and discussion

First, we evaluate the SiB4 COS flux against observations (Sect. 3.1). The accuracy of the ecosystem flux is controlled by
several factors, such as the accuracy in leaf phenology, differences in accuracy of the daytime and nighttime COS vegetation
flux, the accuracy of the soil flux (of both the Berry and Ogée soil model), and the sensitivity to atmospheric COS mole
360 fractions. We discuss the role of each of these factors in the evaluation of SiB4 biosphere fluxes against observations. All
results are based on the standard α values of 1400 and 8862 for C3 and C4 species, respectively. We present COS fluxes
relative to the atmosphere (i.e. negative values indicate uptake by the ecosystem). Next, we study the variability of α_{obs} between
different PFTs and across seasons (Sect. 3.2), to investigate remaining model-data mismatches in the COS vegetation flux that
could potentially be solved by re-calibrating α . Finally, we present global estimates of the COS biospheric sink with different
365 model configurations (Sect. 3.3).

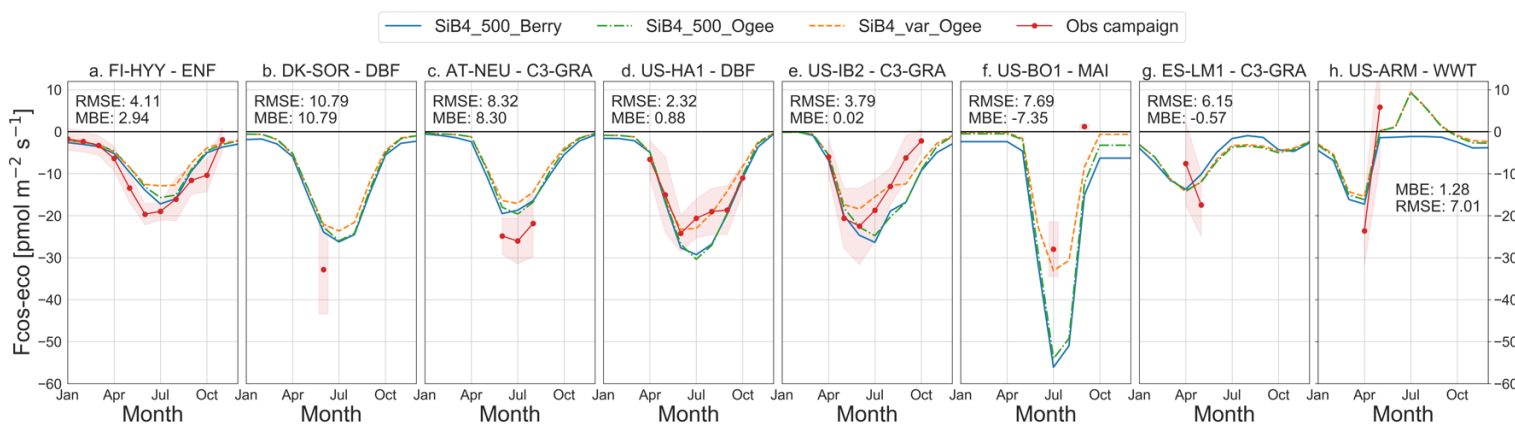
3.1 SiB4 COS flux evaluation and sensitivity

3.1.1 Seasonal variability

Simulated COS ecosystem fluxes capture the seasonal variation of monthly-averaged observations (Fig. 2), with similar results
for vegetation fluxes alone (Fig. S1). Specifically, COS uptake peaked in summer in the simulations, as was observed at the
370 three sites that contain COS flux measurements across different seasons (Fig. 2a, d, e). At the other sites, COS ecosystem
fluxes were only measured during one part of the growing season. Therefore, we also used multi-year NEE, GPP, and latent
heat flux (LE) from FLUXNET, ICOS, and AmeriFlux to evaluate the SiB4 seasonality (Fig S2-4).



Based on the NEE, GPP, and LE observations (Fig. S2-4) the start and end of the growing season are typically well captured
 375 by the SiB4 simulations. The timing and length of the growing season for grassland sites has been previously evaluated by
 Haynes et al. (2019b) using remotely-sensed leaf area index and showed that SiB4 was capable of simulating growing season
 timing and variability across temperature and precipitation gradients. Also, the timing of maximum NEE and GPP, which
 differs by PFT and climatic regions, was well captured; e.g., simulated and observed NEE and GPP peak in spring at the
 savannah grassland site ES-LM1 and at the winter wheat site US-ARM. All other sites show an observed and simulated summer
 380 maximum carbon uptake. Only AT-NEU is an exception, with SiB4 predicting the peak net CO₂ uptake too late into the
 summer compared to the observations, which can be explained by grass cutting that was not included in SiB4. Crop harvesting
 was included in SiB4, but the exact timing was difficult to simulate due to local weather events and considerations other than
 crop ripening. For example, at the US-ARM site the winter wheat harvest was on average simulated at DOY 136 for the years
 2000-2019, close to the actual moment of harvest in 2012: DOY 145. However, for 2012 (the year matching with COS flux
 385 observations), the model simulates harvest almost 4 weeks earlier (DOY 118) than was actually the case, possibly because in
 2012 the meteorological forcing data prescribed generally higher daytime temperatures than observed (the slope between
 observed and model air temperature was 1.14 in 2012), while in other years the model temperatures were similar to
 observations (the slope was on average 1.03 ± 0.04).



390 **Figure 2.** Comparison of ecosystem COS flux seasonal cycles of observations (red) with different SiB4
 model with 500 pmol mol⁻¹ COS and the original Berry soil model (SiB4_500_Berry, blue, solid); a run with variable COS mole
 fractions and the Ogee soil model (SiB4_var_Ogee, orange, dashed); a run with 500 pmol mol⁻¹ COS and the Ogee soil model
 (SiB4_500_Ogee, green, dot-dash). Monthly averages are shown with the 1 σ spread around the mean of observations. Negative
 values indicate uptake of COS by the ecosystem while positive values indicate COS emissions. The model simulations are from the
 395 same year(s) in which observations were made. The MBE and RMSE (pmol m⁻² s⁻¹) are given for monthly average fluxes of the
 SiB4_var_Ogee run. Sites are presented from high to low latitude.



400 For the sites where COS fluxes were only measured in one part of the growing season we assume that the timing of seasonal patterns in COS assimilation were well captured since seasonal patterns in NEE, GPP, and LE are properly simulated (Fig. S2-4) and the model scales the CA activity with V_{max} , and g_s with GPP.

405 We generally found larger underestimations of the ecosystem COS exchange at the higher latitudes (FI-HYY, DK-SOR, AT-NEU, Fig. 2a-c), which is consistent with findings by Ma et al. (2021) who found a missing sink at the higher latitudes that required larger uptake in summer (their Fig. 5b). The model-observation biases that we see in the ecosystem COS fluxes are consistent with biases in GPP for some sites. For example, the underestimation of the COS ecosystem flux at DK-SOR, AT-NEU, and FI-HYY is consistent with underestimations of GPP (Fig. S3a-c), which will be further discussed in Sect. 3.1.3.

3.1.2 Effects of varying atmospheric COS mole fractions

410 Modifying the COS mole fractions to vary spatially and temporally significantly improved the comparison with observations in North America, as seen from the orange (variable COS) and green (fixed COS) line in Fig. 2d-f. Generally, COS mole fractions are lower in the second half of the growing season, leading to lower COS uptake in that period. When a variable COS mole fraction was used, the MBE value in July-August improved from 9.0 to 2.0 $\text{pmol m}^{-2} \text{s}^{-1}$ at US-HA1, from 7.2 to -0.9 $\text{pmol m}^{-2} \text{s}^{-1}$ for US-IB2, and from 28.6 to 5.4 $\text{pmol m}^{-2} \text{s}^{-1}$ in US-BO1. The influence of the COS mole fraction on the biosphere flux was largest at sites within or close to the Corn Belt in Midwestern US with strong biosphere COS uptake (see also Fig. 6) that therefore has the largest summer-time drop in COS mole fractions (Fig. S5d,e) or the lowest COS mole fraction in general (Fig. S5f). The large COS uptake by maize is confirmed by the observed COS fluxes reaching $\sim 70 \text{ pmol m}^{-2} \text{s}^{-1}$ at midday (Fig. S6). In this region, the lower COS mole fractions lead to lower COS uptake, but would in turn lead to a smaller drop in COS mole fractions. As COS uptake and COS mole fractions are interconnected, SiB4 should ideally be directly coupled to an atmospheric transport model.

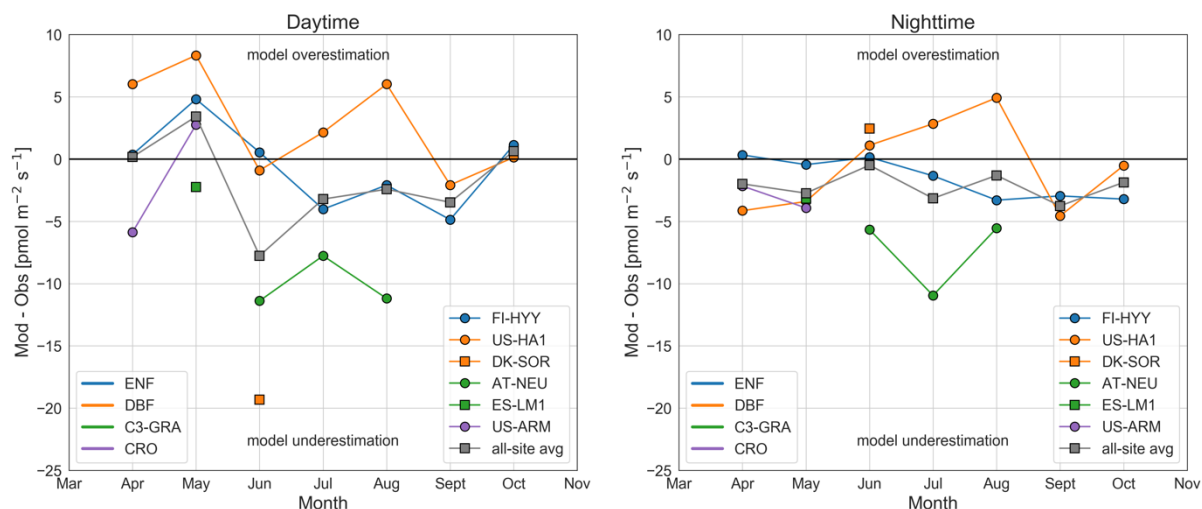
420 At other sites (Europe) the variable COS mole fractions did not improve the model-observation bias, but instead caused a slightly larger underestimation by the model. The comparison of COS mole fractions from the TM5-4DVAR inversion against those observed at the measurement sites (Fig. S5), did not indicate that the COS mole fractions were consistently better simulated over North America than over Europe. These results indicate that the underestimation of COS fluxes over Europe is not likely caused by an underestimation of the COS mole fractions.

425 3.1.3 Diurnal cycles

The monthly average ecosystem COS fluxes (Fig. 2) included both day- and nighttime fluxes, and soil and vegetation fluxes, which may each have its own biases. Figure 3 shows model-observation differences of vegetation COS uptake separated by day- and nighttime, defined as 10 – 15 hr and 21 – 03 hr local time, respectively. These day- and nighttime definitions exclude transitions between day and night (see diurnal cycles in Fig. S6 and S7). On average across all stations, simulated daytime



430 uptake between April through October was $1.9 \pm 6.5 \text{ pmol m}^{-2} \text{ s}^{-1}$ ($= 8 \pm 27 \%$) lower than the observations. Even though the average model-observation difference is small, there is substantial variability between sites. The underestimation of daytime
 435 average (Fig. S3b). However, SiB4 simulates only a 7 % higher GPP in June 2016 compared to the 1996-2018 average. At the same time, LE is overestimated (Fig. S4b). These results point to an underestimation of the RuBisCo and CA enzyme activity, and thus g_{cos} , rather than g_s , as LE is not underestimated but even overestimated. Also at AT-NEU and FI-HYY the underestimation of COS vegetation uptake was consistent with underestimations of simulated GPP against longterm timeseries (Fig. S3a,c), with a 9 % underestimation of the COS vegetation flux and 13 % underestimation of GPP at FI-HYY in the
 440 months June to August. At US-ARM we saw a switch from an underestimation to overestimation of daytime vegetation COS uptake over the months April and May, which may be due to COS emissions from other components than the soil, possibly associated with senescing vegetation, which is currently not represented in SiB4 (nor in other models). Overall, we found large variability in model-observation biases between sites, but no clear distinctions emerge from different PFTs for daytime fluxes.



445

450 **Figure 3. Difference between model simulations and observations of monthly average COS vegetation fluxes (ecosystem – soil) for daytime data (10 – 15 hr local time; left) and nighttime data (21 – 03 hr local time; right). As ecosystem and soil fluxes are needed to obtain the vegetation flux, only sites with these data available are shown here. The model simulations were made with a variable COS mole fraction and the Ogee soil model (SiB4_var_Ogee). Data are colored by PFT.**

The simulated nighttime uptake was on average $2.1 \pm 3.4 \text{ pmol m}^{-2} \text{ s}^{-1}$ ($= 35 \pm 57 \%$) too small. Observed nighttime uptake was on average 25 % of the daytime uptake across sites between May-September, with the largest uptake at AT-NEU ($11.0 \text{ pmol m}^{-2} \text{ s}^{-1}$), ES-LM1 ($6.9 \text{ pmol m}^{-2} \text{ s}^{-1}$), and FI-HYY ($5.9 \text{ pmol m}^{-2} \text{ s}^{-1}$). The small flux values during nighttime make the



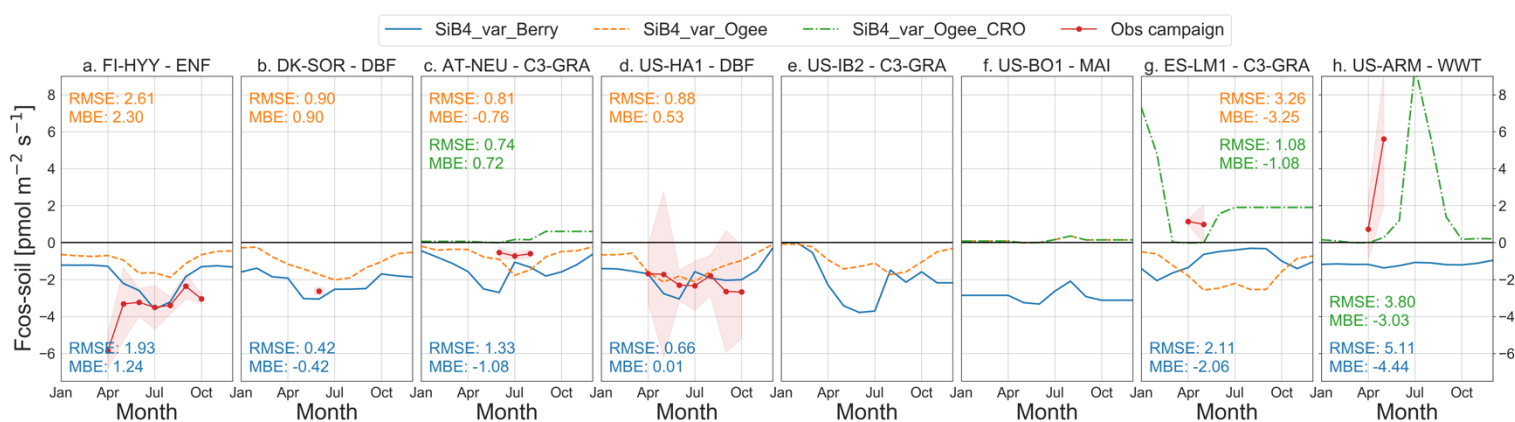
455 model-observation comparison sensitive to the different correction and processing procedures that were used for the different
datasets. Ecosystem fluxes were only storage-corrected for FI-HYY and US-HA1. Kooijmans et al. (2017) showed for FI-
HYY that nighttime storage fluxes were on average $\sim 1 \text{ pmol m}^{-2} \text{ s}^{-1}$ in summer. Additionally, some datasets are filtered based
on a friction velocity threshold, while others are not. Kooijmans et al. (2017) noted that filtering data based on the friction
velocity might bias the data to higher nighttime COS uptake as the uptake can be expected to be limited by the COS gradient
460 at the leaf boundary layer under low turbulence conditions. Given these differences between datasets, and the typically large
random noise of COS flux measurements, the average underestimation may not be significant overall. Still, we found a
substantial underestimation of the nighttime COS uptake at the C3-GRA sites AT-NEU and ES-LM1, and an overestimation
in summer at the DBF sites US-HA1 and DK-SOR. These biases might point to inaccurate minimum stomatal conductance
(g_0) values in SiB4, which are currently set to $10 \text{ mmol m}^{-2} \text{ s}^{-1}$ for all PFTs, except crop types ($40 \text{ mmol m}^{-2} \text{ s}^{-1}$). Observed g_0
465 values at AT-NEU ($10\text{--}65 \text{ mmol m}^{-2} \text{ s}^{-1}$, Wohlfahrt, 2004) are mostly higher than the $10 \text{ mmol m}^{-2} \text{ s}^{-1}$ used in SiB4 and support
the hypothesis that the SiB4 g_0 is too low for this site. Similarly, estimates of g_0 at US-HA1 ($3.1 \text{ mmol m}^{-2} \text{ s}^{-1}$, Wehr et al.
2017) point to a smaller value than used in SiB4 and could explain part of the overestimation of nighttime COS uptake at this
site. These examples show that observations could help to obtain g_0 values for SiB4. Lombardozi et al. (2017) made a literature
overview of reported g_0 values per PFT and showed that g_0 was typically several times larger than the value of $10 \text{ mmol m}^{-2} \text{ s}^{-1}$
470 ¹ currently used in SiB4. We adopted the minimum values of Lombardozi et al. (2017) in SiB4 to test the effect of a modified
 g_0 setting on the nighttime COS vegetation flux (see Table S2 and Fig. S8). Using these updated minimum values, the simulated
nighttime COS uptake for C3-GRA improved at AT-NEU, but had larger biases for other sites and PFTs, especially DBF (Fig
S8). As the g_0 values from Lombardozi et al. (2017) did not consistently improve the nighttime COS uptake we did not adopt
these as standard SiB4 settings.

475 3.1.4 Soil fluxes

The original SiB4 soil model scaled COS soil fluxes to heterotrophic CO_2 respiration, leading to COS uptake rates peaking at
high temperatures in summer (Fig. 4, Fig. S9) and in conditions with sufficient soil moisture (Fig. 4g, Fig. S10g). The Ogée
soil model also simulated COS uptake peaking at high temperatures, and lower uptake rates in winter compared to the Berry
soil model (Fig. 4). In general, the COS uptake simulated by the Berry soil model matched well with observations at forest
480 sites (Fig. 4a, b, d), possibly because their approach was following a study on forest soils (Yi et al. 2007). The Ogée soil model
underestimated the COS uptake at FI-HYY (Fig. 4a), but was closer to observations at the other forest sites US-HA1 and DK-
SOR (Fig. 4b, d). The observed high soil COS uptake in April at FI-HYY is possibly related to snow melt and thawing of the
soil and neither model captures this effect on soil COS exchange.



485 Soil COS emissions were observed at ES-LM1 and US-ARM. US-ARM was an agricultural site where emissions may build up after the peak growing season in the period associated with senescence and harvest (Maseyk et al., 2014). The Berry soil model did not simulate soil COS emissions (Fig. 4h). In contrast, the increase in COS emissions at the agricultural site US-ARM was simulated by the Ogée soil model, although the increase of the emissions started later than in the observations. The soil emissions of COS were not simulated at the C3-GRA site ES-LM1. However, the soil at ES-LM1 was fertilized (Weiner et al. 2018), as well as that AT-NEU (Spielmann et al. 2020), which make these sites more representative of agricultural soils rather than grassland soils. When ES-LM1 was simulated as an agricultural soil (the same code, but with different uptake and production parameter values, see Table 2), the model showed COS emissions more consistent with observations (green line in Fig. 4g). Also, the simulated fluxes at the AT-NEU site became smaller and in better agreement with observations when the site was considered as an agricultural soil.



495 **Figure 4. Comparison of COS soil flux seasonal cycles of observations (red) with different SiB4 model runs: SiB4_var_Berry (blue, solid); SiB4_var_Ogee with the simulation representing the PFT type as indicated in the plot titles (orange, dashed); SiB4_var_Ogee_CRO with the simulation representing agricultural soil (Table 2) for sites AT-NEU, US-BO1, ES-LM1, US-ARM**
 500 **(green, dot-dash). No *in situ* observations of soil COS fluxes are available for US-IB2 and US-BO1. Monthly averages are shown with the 1 σ spread around the mean for observations. The model simulations are from the same year(s) in which observations were made. Negative values indicate uptake of COS by the ecosystem while positive values indicate COS emissions. The MBE and RMSE (pmol m⁻² s⁻¹) are given for monthly average fluxes for all model runs in their respective color. Sites are presented from high to low latitude.**

The accuracy of simulations of soil COS emissions depends on the accuracy of the production parameter a . The standard deviation of the production parameter a (7.3) is relatively large for agricultural soils compared to other soil types (Table 2) and is an indication of the uncertainty of using a single production value in the SiB4 model. Reasons for this uncertainty can be the local variability in soil characteristics like nitrogen content, which has been shown to correlate well with COS production rates (Kaisermann et al. 2018b). Moreover, soil moisture and soil temperature were important parameters in the calculation of the COS soil flux. In general, we found that the variability and absolute values of soil moisture and especially soil temperature were well captured by the SiB4 model. We found a MBE across all sites of 0.01 m³ m⁻³ and 0.1 °C (RMSE 0.06 m³ m⁻³ and 2.1 °C) for soil moisture and temperature, respectively, calculated over all years available from the FLUXNET, AmeriFlux or

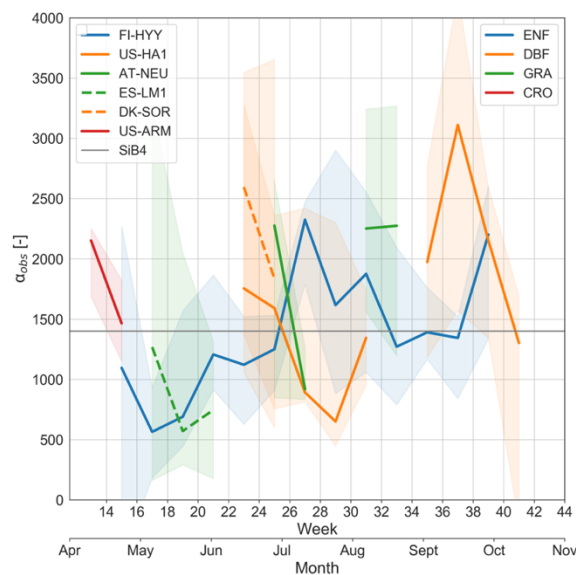


515 ICOS networks. Also, Smith et al. (2020) showed that SiB4 was capable of reproducing the drop in soil moisture as a result of a regional drought in Europe, albeit with a delay. We did not find consistent patterns in model-observation biases of the soil COS fluxes that were consistent with that of soil moisture or temperature (Fig. S9, S10). Still, the soil moisture observations at US-ARM show a sharper drop in spring than the simulations (Fig. S10h), which could explain why the simulations show a delayed onset of soil COS emissions. Moreover, the exact role of thermal and photo-production of COS remains uncertain, as well as the interaction with soil organic matter and litter, and thereby limits the the accuracy of soil COS production simulations (Maseyk et al. 2014; Whelan and Rhew 2015; Meredith et al. 2018; Kaisermann et al. 2018a).

520 Overall, changing from the Berry soil model to the Ogée soil model had a relatively small effect on monthly average ecosystem fluxes (see SiB4_500_Berry (blue) and SiB4_500_Ogee (green) in Fig. 2), except for agricultural sites, where the Berry soil model lacked COS soil emissions that contribute to fluxes at those sites.

3.2 Calibration factor α

525 The calibration factor α was derived to scale g_{cos} to match SiB4 COS plant assimilation with COS flux observations of laboratory leaf gas exchange measurements (Berry et al. 2013). The α_{obs} values that we derived based on field measurements of COS ecosystem and soil fluxes, together with simulated g_{cos} , g_s and g_b , are close to the value 1400 (Fig. 5), which support the initial calibration by Berry et al. (2013) using laboratory leaf gas exchange measurements. At the same time, however, we found α_{obs} to vary in time and between sites (Fig. 5), indicating that a single α value was not able to capture the variation of measured COS vegetation fluxes across sites and seasons. The average summer-time α_{obs} (June-August) of 1616 ± 562 was 15
530 % higher than the current value of 1400. This was consistent with our findings that, on average, SiB4 underestimates COS biosphere fluxes (Sect. 3.1.3). We did not find patterns in α_{obs} that apply to all PFTs in the same way that would have helped to update α in SiB4. However, for DBF and C3-GRA sites we observed that the 2-weekly average α_{obs} typically goes down with increasing air temperature for temperatures above ~ 16 °C (Fig. S11). This observation requires further investigation from hourly data points and will be further discussed in our recommendations (Sect. 4.3).



535

Figure 5. Seasonal change of (2-weekly) median observation-based calibration factor α (α_{obs} ; see Eq. (10)) per site in which colors are separated by PFT. The shaded areas represent the 25th-75th percentiles.

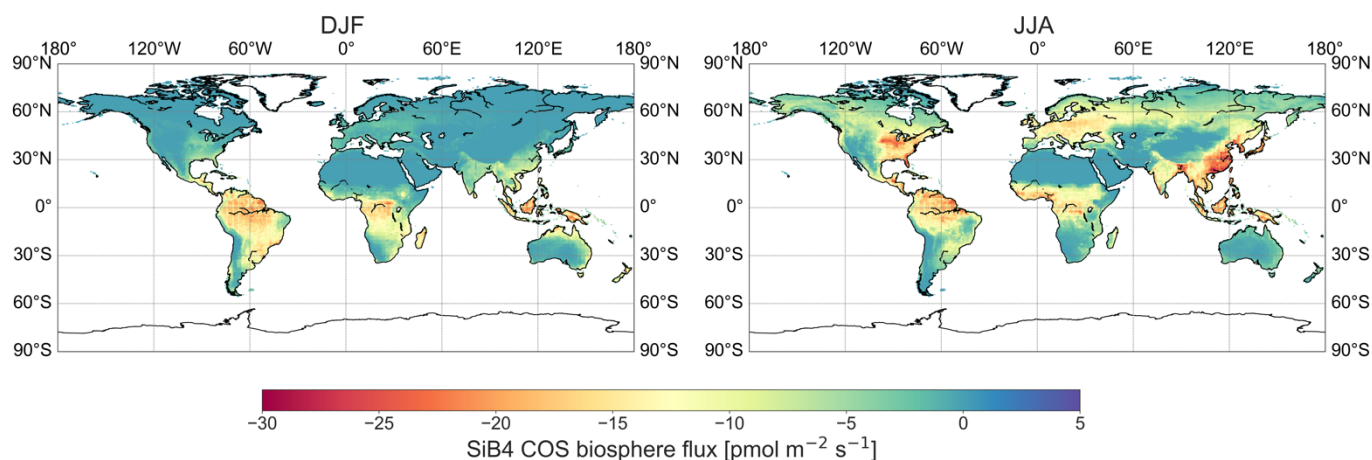
3.3 Global biospheric COS sink

The simulated global patterns in COS uptake were similar to that of GPP (not shown), due to the modeled vegetation COS uptake being coupled to GPP through the RuBisCO enzyme activity and stomatal conductance. Globally, the largest portion of COS uptake took place in tropical regions of South America, Africa, and Asia (Fig 6). In the Northern Hemisphere (NH), COS was mainly taken up during the summer months (Fig. 6b). The spatial distribution of COS uptake was also similar to that presented by Maignan et al. (2021) based on ORCHIDEE simulations. Using the original SiB4 model, i.e., the original Berry soil model and fixed 500 pmol mol⁻¹ COS mole fractions, the global COS biosphere sink amounts to 922 ± 11 Gg S yr⁻¹ over the years 2000-2020 with no substantial trend. 146 Gg S yr⁻¹ out of the total COS biosphere sink was taken up by the soil (Table 1). The change from the original Berry soil model to the Ogée soil model lowered the soil uptake in most regions globally (Fig. 7a, S12). The tropical soil COS uptake reduced from ~ 4-5 pmol m⁻² s⁻¹ to ~ 2-3 pmol m⁻² s⁻¹. In the NH, the soil uptake is also reduced due to the contributions of COS production in agricultural soils. The global COS soil sink thereby reduced from 146 to 104 Gg S yr⁻¹ when we changed from the original Berry soil model to the Ogée soil model, a 29 % reduction of soil uptake, but only a 5 % reduction of the total COS biosphere sink. The modification from a fixed COS mole fraction to spatially and temporally varying COS mole fractions caused an additional reduction of the global COS biosphere sink to 753 Gg S yr⁻¹ (Fig. 7b, S13). This 15 % reduction relative to a simulation with a constant and spatially uniform 500 pmol mol⁻¹ COS mole fraction illustrates the importance of accounting for varying COS mole fractions.



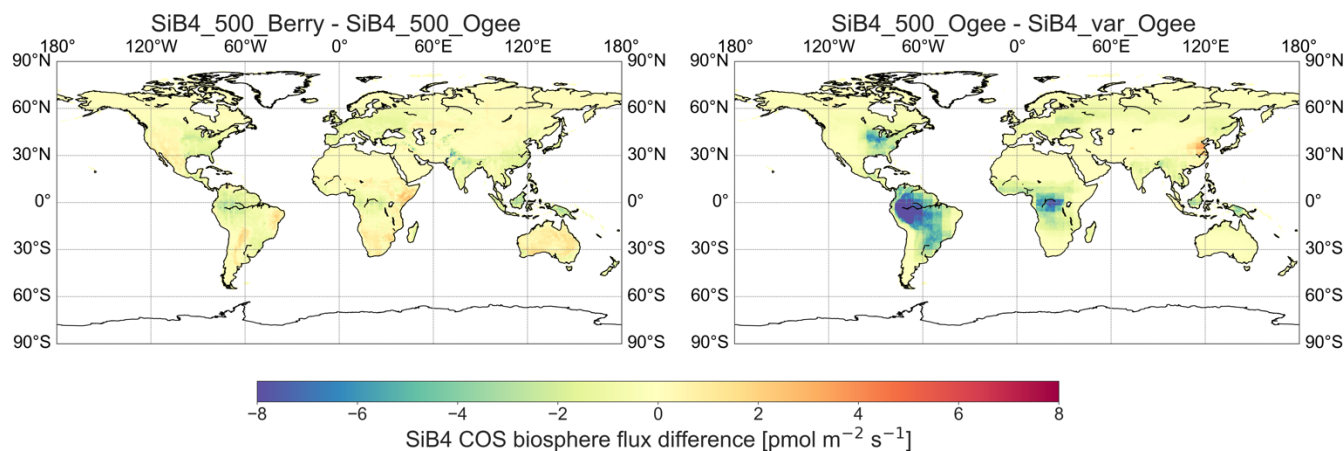
555 The largest drop in the global COS biosphere sink (169 Gg S yr^{-1} , i.e. from 922 to 753 Gg S yr^{-1}) occurs in the tropical regions
(113 Gg S yr^{-1} for latitudes between -23.5 and $+23.5^\circ\text{N}$) as the large biomass in that region leads to the largest COS uptake
and the largest drop in COS mole fractions. This update is a significant contribution to solving the gap in the COS budget of
 $\sim 432 \text{ Gg S yr}^{-1}$ (Ma et al., 2021); however, it does not fully eliminate the missing source in the COS budget. Ma et al. (2021)
showed that assigning the missing COS source to the ocean yields more realistic distributions of COS mole fractions over the
560 tropical regions compared to assuming an overestimated biosphere sink. For these reasons, it is unlikely that the gap in the
COS budget is solely caused by an overestimated tropical biosphere sink. Still, flux observations in the tropics would have to
confirm this.

In Sect. 3.1.3 we found on average an $8 \pm 27\%$ underestimation of the daytime COS vegetation flux as simulated by SiB4. If
565 we assume that the daytime uptake dominates the total COS uptake, and we correct the COS vegetation sink for the
underestimation globally, then we find a vegetation sink of $717 \pm 179 \text{ Gg S yr}^{-1}$ instead of 664 Gg S yr^{-1} , and a total biosphere
uptake of $806 \pm 179 \text{ Gg S yr}^{-1}$ instead of 753 Gg S yr^{-1} . Note, however, that this scaling is highly uncertain, because we found
substantial variability between sites, and a large fraction of the uptake occurs in the tropics, for which we cannot validate the
SiB4 model due to a lack of observations.



570

Figure 6. Global distribution of the COS biosphere flux in winter (DJF, left) and summer months (JJA, right) as simulated by SiB4_var_Ogee over the years 2000-2020. Negative values indicate uptake of COS by the biosphere while positive values indicate COS emissions.



575 **Figure 7. COS biosphere flux difference between two SiB4 model runs. Left: difference between SiB4_500_Berry and SiB4_500_Ogee to show the flux difference between the soil models. Right: difference between the SiB4_500_Ogee and SiB4_var_Ogee to show the effect of changing to variable mole fractions. Negative values indicate a drop in the biosphere COS uptake.**

4. Recommendations for COS-specific future model development

580 We found model-observation biases that could be ascribed to different components of the model (depending on the site), such as the soil COS flux or vegetation COS uptake, where the latter was caused by underestimated enzyme activity that also links to GPP. If sufficient COS flux observations were available, these could help as an extra constraint to improve the model enzyme activity and thereby GPP. Such an approach would require a number of advancements in the understanding and implementation of COS biosphere exchange in SiB4. We have identified a number of ways to improve the COS flux
585 simulations in SiB4, which might also apply to mechanistic COS implementations in other biosphere models:

1. Based on the analysis of the calibration factor α_{obs} (Sect. 3.2) **we suggest a refined calibration of the internal conductance g_{cos} such that it captures the true temperature variation of COS vegetation fluxes.** The current calibration factor of 1400 is based on laboratory leaf gas exchange measurements of different plant species. However, our analysis based on field observations of COS vegetation fluxes shows that an alpha of 1400 mostly underestimates the COS uptake, and suggest that the laboratory-based calibration did not fully resemble the COS vegetation uptake
590 in the field. We suggest a re-calibration of g_{cos} based on both laboratory and field observations of the COS vegetation uptake. Extra attention should be given to the temperature response of COS uptake. The modeled COS uptake is strongly coupled to GPP. However, several studies have shown that the ratio of COS to CO_2 deposition velocities (in literature also called the leaf relative uptake ratio) varies with temperature (Cochavi et al., 2021; Stimler et al., 2010)
595 and humidity (Sun et al. 2018; Kooijmans et al. 2019), in addition to the better known variability with light. The temperature response of the COS uptake is currently taken from V_{max} and is scaled with an empirical temperature function (Eq. (2)) and an additional factor T_{can}/T_0 (Eq. (3)), where the latter increases the COS uptake at higher temperatures. However, the T_{can}/T_0 term has been added as a simple correction, but has not been empirically derived.



- 600 The temperature dependence of the CA enzyme activity could be determined from laboratory experiments, to be able to keep other effects (e.g. on mesophyll conductance) than temperature constant. Field observations could then be used to scale the laboratory-based calibration to ecosystem level and to different PFTs.
2. The SiB4 model is capable of simulating nighttime COS vegetation uptake through stomatal opening, although the nighttime uptake was often underestimated (Fig. 3). **As nighttime COS vegetation uptake is driven by stomatal opening, the COS flux observations can be used to estimate nighttime (minimum) stomatal conductance values** (Berkelhammer et al., 2020; Maignan et al., 2021; Wehr et al., 2017). These values can be compared against those summarized by Lombardozi et al. (2017) and tested in SiB4. However, **similar approaches and processing techniques are required to be able to evaluate the accuracy of the nighttime COS uptake and determine the nighttime stomatal conductance.** Changing the minimum stomatal conductance values would also have consequences for simulations of daytime carbon, water, and energy, which should also be (re-)evaluated.
 - 610 3. We have seen that the simulated COS soil flux can be very different depending on biome (in SiB4 selected as the PFT). This is especially true for fertilized soils that are typically found in agricultural sites, where large emissions of COS are observed. However, soils can contain high nitrogen contents regardless of whether or not it is an agricultural soil. Therefore, it is important to know the nitrogen content for setting the soil COS uptake and production parameter values for the COS soil flux calculation (Table 2). **We suggest the use of global maps of the soil nitrogen content and to use the relation between COS soil production and soil nitrogen content (Kaisermann et al. 2018b) for more accurate COS soil production simulations.**
 - 615 4. This study relied on the availability of field observations. We were able to evaluate SiB4 with the COS field observations available from a number of PFTs. **However, we lacked observations on evergreen broadleaf forests that are largely represented in tropical regions. Such observations could give further insights into the COS budget in tropical regions, where currently the largest uncertainties exist.** Moreover, controlled laboratory measurements of soil COS exchange have been shown to be very powerful to understand the soil COS exchange and to parameterize COS soil models (Meredith et al., 2018, 2019). However, field observations of COS soil exchange along with ecosystem COS fluxes are needed to evaluate COS soil models under field conditions (Ogée et al., 2016; Sun et al., 2015), which would also require standardization of measurement and processing techniques (Kohonen et al., 2020). Finally, the NOAA measurement network of atmospheric COS mole fractions has good coverage over
620 North America and the Pacific Ocean, but other regions are less well represented. The COS mole fraction fields that we prescribed to the SiB4 model rely on the availability of COS observations. A better global coverage of COS mole fraction observations would therefore be beneficial, e.g. through the use of satellite data, where sensitivity to the middle and upper troposphere can currently be achieved (Glatthor et al. 2015; Kuai et al. 2014). Moreover, SiB4
625 should ideally be directly coupled to an atmospheric transport model to account for the interconnection between COS uptake and COS mole fractions.
- 630



Conclusion

635 The experimental efforts made in the last decade to obtain field observations of COS ecosystem fluxes, now offer the possibility of a unique SiB4 model validation of COS biosphere exchange over different biomes. SiB4 was demonstrated to be capable of simulating the diurnal and seasonal variation of COS fluxes in the boreal, temperate and Mediterranean region, however with an average underestimation of $8 \pm 27\%$ of the daytime vegetation flux. The magnitude of the biases differed per site, but could not be ascribed to a single component of the model.

640 We find a lower global soil COS sink with the implementation of the Ogée et al. (2016) soil COS model. Still, the soil COS flux remains a relatively small component in the total COS budget, which benefits the use of COS as a global photosynthesis tracer. A larger effect on the global COS biosphere sink was found by changing the fixed COS mole fraction of $500 \text{ pmol mol}^{-1}$ to values that vary spatially and temporally. The reduction in the COS sink strength is most pronounced in regions with large biomass such as the tropics. This analysis highlights the importance of accounting for variations in atmospheric COS mole
645 fractions, which was not yet adopted as a standard practice.

We make a number of recommendations for future improvements of the model, including re-calibration of the COS model parameters. However, we are limited by data coverage to be able to accurately constrain the model over different PFTs and seasons. More campaigns and long-term observations in underrepresented PFTs, biomes and soil types would be key to
650 continued improvement of the model.

Code and data availability

The SiB4 code is available online at https://gitlab.com/kdhaynes/sib4_corral. SiB4 simulation output used in this study is available at <https://doi.org/10.5281/zenodo.5084644>. COS campaign data are downloaded from the original data publications as reported in Table 3. Long-term CO₂ flux timeseries from FLUXNET, AmeriFlux or ICOS are downloaded from the
655 references listed in Table S1.

Author contributions

LMJK and MK devised the study. LMJK and AC implemented the COS model developments with help from AK, IB, KH, JO, LM, and WS. LMJK, AK, KH, IB, ITL, MG, WP and JM developed the procedure for running SiB4 simulations. LMJK analysed the results with consultation of AC and MK. JM performed TM5 model inversion runs. WS, KMK, TV, IM, HC, FS,
660 GW, MB, MW, KM, US, RC, and RW provided data and site-specific insights. LMJK wrote the manuscript and all authors provided comments.



Competing interests

The authors declare that they have no conflict of interest

Acknowledgement

665 We thank everyone that contributed to the collection of data through campaigns as well as the FLUXNET, AmeriFlux and
ICOS network. Specifically, we acknowledge the Alexander von Humboldt Foundation for supporting the MANIP project
with the Max-Planck Prize to Markus Reichstein that was used for the collection of ICOS data at ES-LM1. Data collection at
FI-HYY was supported by ICOS-Finland (319871) and The Atmosphere and Climate Competence Center (ACCC) Flagship,
funded by the Academy of Finland (grant number 337549). Data from the Sorø beech forest site (DK-SOR) have been
670 measured, evaluated and provided by Kim Pilegaard and Andreas Ibrom and the station team. The work was funded by the
Technical University of Denmark (DTU), the Danish Research Council (DFF – 1323-00182), the Danish Ministry of higher
Education and Science (5072-00008B) and the EU research infrastructure projects RINGO and ICOS. Operation of the US-
HA1 site is supported by the AmeriFlux Management Project with funding by the U.S. Department of Energy’s Office of
Science under Contract No. DE-AC02-05CH11231, and additionally is a part of the Harvard Forest LTER site supported by
675 the National Science Foundation (DEB-1832210). Data collection at US-ARM was supported by the Office of Biological and
Environmental Research of the US Department of Energy under contract No. DE-AC02-05CH11231 as part of the
Atmospheric Radiation Measurement Program (ARM). We are very grateful to the principal investigators J. William Munger
(US-HA1), Sebastien Biraud (US-ARM), Roser Matamala, David Cook (US-IB2), Tilden Meyers (US-BO1), Andreas Ibrom
(DK-SOR) and Mirco Migliavacca (ES-LM1)

680 Financial support

This work was funded through the ERC-advanced funding scheme (AdG 2016 Project Number: 742798, Project Acronym:
COS-OCS). SiB4 simulations were performed using a grant for computing time (17616) from NWO. TV was supported by
the grant of the Tyumen region, Russia, Government in accordance with the Program of the World-Class West Siberian
Interregional Scientific and Educational Center (National Project “Nauka”). IM was supported by ICOS Finland and ACCC
685 Flagship funded by the Academy of Finland grant number 337549. GW and FS received funding from the Austrian National
Science Fund (FWF) through grants P27176, P31669 and I3859.

References

Asaf, D., Rotenberg, E., Tatarinov, F., Dicken, U., Montzka, S. A. and Yakir, D.: Ecosystem photosynthesis inferred from
measurements of carbonyl sulphide flux, *Nat. Geosci.*, 6(3), 186–190, doi:10.1038/ngeo1730, 2013.



- 690 Badger, M. R. and Price, G. D.: The Role of Carbonic Anhydrase in Photosynthesis, *Annu. Rev. Plant Physiol. Plant Mol. Biol.*, 45(1), 369–392, doi:10.1146/annurev.pp.45.060194.002101, 1994.
- Baker, I., Denning, S. and Stöckli, R.: North American gross primary productivity: regional characterization and interannual variability, *Tellus B Chem. Phys. Meteorol.*, 62(5), 533–549, doi:10.1111/j.1600-0889.2010.00492.x, 2010.
- Berkelhammer, M., Alsip, B., Matamala, R., Cook, D., Whelan, M. E., Joo, E., Bernacchi, C., Miller, J. and Meyers, T.:
695 Seasonal Evolution of Canopy Stomatal Conductance for a Prairie and Maize Field in the Midwestern United States from Continuous Carbonyl Sulfide Fluxes, *Geophys. Res. Lett.*, 47(6), e2019GL085652, doi:https://doi.org/10.1029/2019GL085652, 2020.
- Berry, J., Wolf, A., Campbell, J. E., Baker, I., Blake, N., Blake, D., Denning, A. S., Kawa, S. R., Montzka, S. A., Seibt, U., Stimler, K., Yakir, D. and Zhu, Z.: A coupled model of the global cycles of carbonyl sulfide and CO₂: A possible
700 new window on the carbon cycle, *J. Geophys. Res. Biogeosciences*, 118(2), 842–852, doi:10.1002/jgrg.20068, 2013.
- Campbell, J. E., Berry, J. A., Seibt, U., Smith, S. J., Montzka, S. A., Launois, T., Belviso, S., Bopp, L. and Laine, M.: Large historical growth in global terrestrial gross primary production, *Nature*, 544, 84, doi:10.1038/nature22030, 2017.
- Cochavi, A., Amer, M., Stern, R., Tatarinov, F., Migliavacca, M. and Yakir, D.: Differential responses to two heatwave
705 intensities in a Mediterranean citrus orchard are identified by combining measurements of fluorescence and carbonyl sulfide (COS) and CO₂ uptake, *New Phytol.*, 230, 1394–1406, doi:10.1111/nph.17247, 2021.
- Collatz, G. J., Ribas-Carbo, M. and Berry, J. A.: Coupled Photosynthesis-Stomatal Conductance Model for Leaves of C₄ Plants, *Funct. Plant Biol.*, 19(5), 519–538, doi:10.1071/PP9920519, 1992.
- Commane, R., Meredith, L. K., Baker, I. T., Berry, J. A., Munger, J. W., Montzka, S. A., Templer, P. H., Juice, S. M., Zahniser, M. S. and Wofsy, S. C.: Seasonal fluxes of carbonyl sulfide in a midlatitude forest, *P. Natl. Acad. Sci. USA*, 112(46),
710 14162–14167, doi:10.1073/pnas.1504131112, 2015.
- Deepagoda, T. K. K. C., Moldrup, P., Schjønning, P., de Jonge, L. W., Kawamoto, K. and Komatsu, T.: Density-Corrected Models for Gas Diffusivity and Air Permeability in Unsaturated Soil, *Vadose Zo. J.*, 10(1), 226–238, doi:10.2136/vzj2009.0137, 2011.
- Van Diest, H. and Kesselmeier, J.: Soil atmosphere exchange of carbonyl sulfide (COS) regulated by diffusivity depending
715 on water-filled pore space, *Biogeosciences*, 5(2), 475–483, doi:10.5194/bg-5-475-2008, 2008.
- Elliott, S., Lu, E. and Rowland, F. S.: Rates and mechanisms for the hydrolysis of carbonyl sulfide in natural waters, *Environ. Sci. Technol.*, 23(4), 458–461, doi:10.1021/es00181a011, 1989.
- Evans, J. R., Caemmerer, S. V., Setchell, B. A. and Hudson, G. S.: The Relationship Between CO₂ Transfer Conductance and Leaf Anatomy in Transgenic Tobacco With a Reduced Content of Rubisco, *Funct. Plant Biol.*, 21(4), 475–495,
720 doi:10.1071/PP9940475, 1994.
- Gelaro, R., McCarty, W., Suárez, M. J., Todling, R., Molod, A., Takacs, L., Randles, C. A., Darmenov, A., Bosilovich, M. G., Reichle, R., Wargan, K., Coy, L., Cullather, R., Draper, C., Akella, S., Buchard, V., Conaty, A., da Silva, A. M., Gu, W., Kim, G.-K., Koster, R., Lucchesi, R., Merkova, D., Nielsen, J. E., Partyka, G., Pawson, S., Putman, W.,



- 725 Rienecker, M., Schubert, S. D., Sienkiewicz, M. and Zhao, B.: The Modern-Era Retrospective Analysis for Research and Applications, Version 2 (MERRA-2), *J. Clim.*, 30(14), 5419–5454, doi:10.1175/JCLI-D-16-0758.1, 2017.
- Glatthor, N., Höpfner, M., Baker, I. T., Berry, J., Campbell, J. E., Kawa, S. R., Krysztofiak, G., Leyser, A., Sinnhuber, B. M., Stiller, G. P., Stinecpher, J. and Von Clarmann, T.: Tropical sources and sinks of carbonyl sulfide observed from space, *Geophys. Res. Lett.*, 42(22), 10082–10090, doi:10.1002/2015GL066293, 2015.
- Haynes, K., Baker, I. and Denning, S.: Simple Biosphere Model version 4.2 (SiB4) Technical Description, Mountain Scholar, Colorado State University, Fort Collins, CO, USA. [online] Available from: <https://hdl.handle.net/10217/200691>, 2020.
- 730 Haynes, K. D., Baker, I. T., Denning, A. S., Stöckli, R., Schaefer, K., Lokupitiya, E. Y. and Haynes, J. M.: Representing Grasslands Using Dynamic Prognostic Phenology Based on Biological Growth Stages: 1. Implementation in the Simple Biosphere Model (SiB4), *J. Adv. Model. Earth Syst.*, 11(12), 4423–4439, doi:10.1029/2018MS001540, 2019a.
- 735 Haynes, K. D., Baker, I. T., Denning, A. S., Wolf, S., Wohlfahrt, G., Kiely, G., Minaya, R. C. and Haynes, J. M.: Representing Grasslands Using Dynamic Prognostic Phenology Based on Biological Growth Stages: Part 2. Carbon Cycling, *J. Adv. Model. Earth Syst.*, 11(12), 4440–4465, doi:10.1029/2018MS001541, 2019b.
- Huffman, G. J., Adler, R. F., Morrissey, M. M., Bolvin, D. T., Curtis, S., Joyce, R., McGavock, B. and Susskind, J.: Global Precipitation at One-Degree Daily Resolution from Multisatellite Observations, *J. Hydrometeorol.*, 2(1), 36–50, doi:10.1175/1525-7541(2001)002<0036:GPAODD>2.0.CO;2, 2001.
- 740 Kaisermann, A., Ogée, J., Sauze, J., Wohl, S., Jones, S. P., Gutierrez, A. and Wingate, L.: Disentangling the rates of carbonyl sulphide (COS) production and consumption and their dependency with soil properties across biomes and land use types, *Atmos. Chem. Phys.*, 18, 9425–9440, doi:10.5194/acp-2017-1229, 2018a.
- 745 Kaisermann, A., Jones, S. P., Wohl, S., Ogée, J. and Wingate, L.: Nitrogen Fertilization Reduces the Capacity of Soils to Take up Atmospheric Carbonyl Sulphide, *Soil Syst.*, 2(4), doi:10.3390/soilsystems2040062, 2018b.
- Kesselmeier, J., Teusch, N. and Kuhn, U.: Controlling variables for the uptake of atmospheric carbonyl sulfide by soil, *J. Geophys. Res. Atmos.*, 104(D9), 11577–11584, doi:10.1029/1999JD900090, 1999.
- Kettle, A. J., Kuhn, U., von Hobe, M., Kesselmeier, J. and Andreae, M. O.: Global budget of atmospheric carbonyl sulfide: 750 Temporal and spatial variations of the dominant sources and sinks, *J. Geophys. Res.-Atmos.*, 107, 4658, doi:10.1029/2002JD002187, 2002.
- Kohonen, K.-M., Kolari, P., Kooijmans, L. M. J., Chen, H., Seibt, U., Sun, W. and Mammarella, I.: Towards standardized processing of eddy covariance flux measurements of carbonyl sulfide, *Atmos. Meas. Tech.*, 13(7), 3957–3975, doi:10.5194/amt-13-3957-2020, 2020.
- 755 Kooijmans, L. M. J., Maseyk, K., Seibt, U., Sun, W., Vesala, T., Mammarella, I., Kolari, P., Aalto, J., Franchin, A., Vecchi, R., Valli, G. and Chen, H.: Canopy uptake dominates nighttime carbonyl sulfide fluxes in a boreal forest, *Atmos. Chem. Phys.*, 17, 11453–11465, doi:10.5194/acp-17-11453-2017, 2017.



- Kooijmans, L. M. J. J., Sun, W., Aalto, J., Erkkilä, K.-M. M., Maseyk, K., Seibt, U., Vesala, T., Mammarella, I. and Chen, H.: Influences of light and humidity on carbonyl sulfide-based estimates of photosynthesis, *Proc. Natl. Acad. Sci. U. S. A.*, 116(7), 2470–2475, doi:10.1073/pnas.1807600116, 2019.
- 760 Kuai, L., Worden, J., Kulawik, S. S., Montzka, S. A. and Liu, J.: Characterization of Aura TES carbonyl sulfide retrievals over ocean, *Atmos. Meas. Tech.*, 7, 163–172, doi:10.5194/amt-7-163-2014, 2014.
- Kuai, L., Worden, J. R., Campbell, J. E., Kulawik, S. S., Li, K.-F. F., Lee, M., Weidner, R. J., Montzka, S. A., Moore, F. L., Berry, J. A., Baker, I., Denning, A. S., Bian, H., Bowman, K. W., Liu, J. and Yung, Y. L.: Estimate of carbonyl sulfide tropical oceanic surface fluxes using aura tropospheric emission spectrometer observations, *J. Geophys. Res.*, 120(20), 11,11-12,23, doi:10.1002/2015JD023493, 2015.
- 765 Launois, T., Belviso, S., Bopp, L., Fichot, C. G. and Peylin, P.: A new model for the global biogeochemical cycle of carbonyl sulfide – Part 1: Assessment of direct marine emissions with an oceanic general circulation and biogeochemistry model, *Atmos. Chem. Phys.*, 15(5), 2295–2312, doi:10.5194/acp-15-2295-2015, 2015a.
- 770 Launois, T., Peylin, P., Belviso, S. and Poulter, B.: A new model of the global biogeochemical cycle of carbonyl sulfide - Part 2: Use of carbonyl sulfide to constrain gross primary productivity in current vegetation models, *Atmos. Chem. Phys.*, 15(16), 9285–9312, doi:10.5194/acp-15-9285-2015, 2015b.
- Lawrence, D. M. and Slater, A. G.: Incorporating organic soil into a global climate model, *Clim. Dyn.*, 30(2), 145–160, doi:10.1007/s00382-007-0278-1, 2008.
- 775 Lawrence, P. J. and Chase, T. N.: Representing a new MODIS consistent land surface in the Community Land Model (CLM 3.0), *J. Geophys. Res. Biogeosciences*, 112(G1), doi:10.1029/2006JG000168, 2007.
- Lennartz, S. T., Marandino, C. A., von Hobe, M., Cortes, P., Quack, B., Simo, R., Booge, D., Pozzer, A., Steinhoff, T., Arevalo-Martinez, D. L., Kloss, C., Bracher, A., Rottgers, R., Atlas, E. and Kruger, K.: Direct oceanic emissions unlikely to account for the missing source of atmospheric carbonyl sulfide, *Atmos. Chem. Phys.*, 17(1), 385–402, doi:10.5194/acp-17-385-2017, 2017.
- 780 Lennartz, S. T., von Hobe, M., Booge, D., Bittig, H., Fischer, T., Gonçalves-Araujo, R., Ksionzek, K. B., Koch, B. P., Bracher, A., Röttgers, R., Quack, B. and Marandino, C. A.: The influence of dissolved organic matter on the marine production of carbonyl sulfide (OCS) and carbon disulfide (CS₂) in the Eastern Tropical South Pacific, *Ocean Sci.*, 15, 1071–1090, doi:doi.org/10.5194/os-15-1071-2019, 2019.
- 785 Lokupitiya, E., Denning, S., Paustian, K., Baker, I., Schaefer, K., Verma, S., Meyers, T., Bernacchi, C. J., Suyker, A. and Fischer, M.: Incorporation of crop phenology in Simple Biosphere Model (SiBcrop) to improve land-atmosphere carbon exchanges from croplands, *Biogeosciences*, 6(6), 969–986, doi:10.5194/bg-6-969-2009, 2009.
- Lombardozzi, D. L., Zeppel, M. J. B., Fisher, R. A. and Tawfik, A.: Representing nighttime and minimum conductance in CLM4.5: global hydrology and carbon sensitivity analysis using observational constraints, *Geosci. Model Dev.*, 10(1), 321–331, doi:10.5194/gmd-10-321-2017, 2017.
- 790 Ma, J., Kooijmans, L. M. J., Cho, A., Montzka, S. A., Glatthor, N., Worden, J. R., Kuai, L., Atlas, E. L. and Krol, M. C.:



- Inverse modelling of carbonyl sulfide: implementation, evaluation and implications for the global budget, *Atmos. Chem. Phys.*, 21(5), 3507–3529, doi:10.5194/acp-21-3507-2021, 2021.
- 795 Maignan, F., Abadie, C., Remaud, M., Kooijmans, L. M. J., Kohonen, K.-M., Commane, R., Wehr, R., Campbell, J. E., Belviso, S., Montzka, S. A., Raoult, N., Seibt, U., Shiga, Y. P., Vuichard, N., Whelan, M. E. and Peylin, P.: Carbonyl Sulfide: Comparing a Mechanistic Representation of the Vegetation Uptake in a Land Surface Model and the Leaf Relative Uptake Approach, *Biogeosciences*, 18(9), 2917–2955, doi:10.5194/bg-18-2917-2021, 2021.
- Maseyk, K., Berry, J. A., Billesbach, D., Campbell, J. E., Torn, M. S., Zahniser, M. and Seibt, U.: Sources and sinks of carbonyl sulfide in an agricultural field in the Southern Great Plains, *P. Natl. Acad. Sci. USA*, 111(25), 9064–9069, 800 doi:10.1073/pnas.1319132111, 2014.
- Meredith, L. K., Boye, K., Youngerman, C., Whelan, M., Ogée, J., Sauze, J. and Wingate, L.: Coupled Biological and Abiotic Mechanisms Driving Carbonyl Sulfide Production in Soils, *Soil Syst.*, 2(3), doi:10.3390/soilsystems2030037, 2018.
- Meredith, L. K., Ogée, J., Boye, K., Singer, E., Wingate, L., von Sperber, C., Sengupta, A., Whelan, M., Pang, E., Keiluweit, M., Brüggemann, N., Berry, J. A. and Welander, P. V.: Soil exchange rates of COS and CO₁₈O differ with the 805 diversity of microbial communities and their carbonic anhydrase enzymes, *ISME J.*, 13(2), 290–300, doi:10.1038/s41396-018-0270-2, 2019.
- Millington, R. J. and Quirk, J. P.: Permeability of porous solids, *Trans. Faraday Soc.*, 57(0), 1200–1207, doi:10.1039/TF9615701200, 1961.
- Montzka, S. A., Calvert, P., Hall, B. D., Elkins, J. W., Conway, T. J., Tans, P. P. and Sweeney, C.: On the global distribution, 810 seasonality, and budget of atmospheric carbonyl sulfide (COS) and some similarities to CO₂, *J. Geophys. Res.-Atmos.*, 112(D9), D09302, doi:10.1029/2006JD007665, 2007.
- Ogée, J., Sauze, J., Kesselmeier, J., Genty, B., Van Diest, H., Launois, T. and Wingate, L.: A new mechanistic framework to predict OCS fluxes from soils, *Biogeosciences*, 13(8), 2221–2240, doi:10.5194/bg-13-2221-2016, 2016.
- Pastorello, G., Trotta, C., Canfora, E., Chu, H., Christianson, D., Cheah, Y.-W., Poindexter, C., Chen, J., Elbashandy, A., 815 Humphrey, M., Isaac, P., Polidori, D., Reichstein, M., Ribeca, A., van Ingen, C., Vuichard, N., Zhang, L., Amiro, B., Ammann, C., Arain, M. A., Ardö, J., Arkebauer, T., Arndt, S. K., Arriga, N., Aubinet, M., Aurela, M., Baldocchi, D., Barr, A., Beamesderfer, E., Marchesini, L. B., Bergeron, O., Beringer, J., Bernhofer, C., Berveiller, D., Billesbach, D., Black, T. A., Blanken, P. D., Bohrer, G., Boike, J., Bolstad, P. V., Bonal, D., Bonnefond, J.-M., Bowling, D. R., Bracho, R., Brodeur, J., Brümmer, C., Buchmann, N., Burban, B., Burns, S. P., Buysse, P., Cale, P., 820 Cavagna, M., Cellier, P., Chen, S., Chini, I., Christensen, T. R., Cleverly, J., Collalti, A., Consalvo, C., Cook, B. D., Cook, D., Coursolle, C., Cremonese, E., Curtis, P. S., D’Andrea, E., da Rocha, H., Dai, X., Davis, K. J., Cinti, B. De, Grandcourt, A. de Ligne, A. De, De Oliveira, R. C., Delpierre, N., Desai, A. R., Di Bella, C. M., Tommasi, P. di, Dolman, H., Domingo, F., Dong, G., Dore, S., Duce, P., Dufrière, E., Dunn, A., Dušek, J., Eamus, D., Eichelmann, U., ElKhidir, H. A. M., Eugster, W., Ewenz, C. M., Ewers, B., Famulari, D., Fares, S., Feigenwinter, I., Feitz, A., 825 Fensholt, R., Filippa, G., Fischer, M., Frank, J., Galvagno, M., et al.: The FLUXNET2015 dataset and the ONEFlux



- processing pipeline for eddy covariance data, *Sci. Data*, 7(1), 225, doi:10.1038/s41597-020-0534-3, 2020.
- Seibt, U., Kesselmeier, J., Sandoval-Soto, L., Kuhn, U. and Berry, J. A.: A kinetic analysis of leaf uptake of COS and its relation to transpiration, photosynthesis and carbon isotope fractionation, *Biogeosciences*, 7(1), 333–341, doi:10.5194/bg-7-333-2010, 2010.
- 830 Sellers, P. J., Berry, J. A., Collatz, G. J., Field, C. B. and Hall, F. G.: Canopy reflectance, photosynthesis, and transpiration. III. A reanalysis using improved leaf models and a new canopy integration scheme., *Remote Sens. Environ.*, 42(3), 187–216, doi:10.1016/0034-4257(92)90102-P, 1992.
- Sellers, P. J., Randall, D. A., Collatz, G. J., Berry, J. A., Field, C. B., Dazlich, D. A., Zhang, C., Collelo, G. D. and Bounoua, L.: A Revised Land Surface Parameterization (SiB2) for Atmospheric GCMS. Part I: Model Formulation, *J. Clim.*, 9(4), 676–705, doi:10.1175/1520-0442(1996)009<0676:ARLSPF>2.0.CO;2, 1996.
- 835 Smith, N. E., Kooijmans, L. M. J., Koren, G., van Schaik, E., van der Woude, A. M., Wanders, N., Ramonet, M., Xueref-Remy, I., Siebicke, L., Manca, G., Brümmner, C., Baker, I. T., Haynes, K. D., Luijkx, I. T. and Peters, W.: Spring enhancement and summer reduction in carbon uptake during the 2018 drought in northwestern Europe, *Philos. Trans. R. Soc. B Biol. Sci.*, 375(1810), 20190509, doi:10.1098/rstb.2019.0509, 2020.
- 840 Spielmann, F. M., Wohlfahrt, G., Hammerle, A., Kitz, F., Migliavacca, M., Alberti, G., Ibrom, A., El-Madany, T. S., Gerdel, K., Moreno, G., Kolle, O., Karl, T., Peressotti, A. and Delle Vedove, G.: Gross Primary Productivity of Four European Ecosystems Constrained by Joint CO₂ and COS Flux Measurements, *Geophys. Res. Lett.*, 46(10), 5284–5293, doi:10.1029/2019GL082006, 2019.
- Spielmann, F. M., Hammerle, A., Kitz, F., Gerdel, K. and Wohlfahrt, G.: Seasonal dynamics of the COS and CO₂ exchange of a managed temperate grassland, *Biogeosciences*, 17(16), 4281–4295, doi:10.5194/bg-17-4281-2020, 2020.
- 845 Stimler, K., Montzka, S. A., Berry, J. A., Rudich, Y. and Yakir, D.: Relationships between carbonyl sulfide (COS) and CO₂ during leaf gas exchange, *New Phytol.*, 186(4), 869–878, doi:10.1111/j.1469-8137.2010.03218.x, 2010.
- Stimler, K., Berry, J. A., Montzka, S. A. and Yakir, D.: Association between Carbonyl Sulfide Uptake and $\delta^{18}O$ during Gas Exchange in C₃ and C₄ Leaves, *Plant Physiol.*, 157(1), 509–517, doi:10.1104/pp.111.176578, 2011.
- 850 Sun, W., Maseyk, K., Lett, C. and Seibt, U.: A soil diffusion–reaction model for surface COS flux: COSSM v1, *Geosci. Model Dev.*, 8(10), 3055–3070, doi:10.5194/gmd-8-3055-2015, 2015.
- Sun, W., Kooijmans, L. M. J., Maseyk, K., Chen, H., Mammarella, I., Vesala, T., Levula, J., Keskinen, H. and Seibt, U.: Soil fluxes of carbonyl sulfide (COS), carbon monoxide, and carbon dioxide in a boreal forest in southern Finland, *Atmos. Chem. Phys.*, 18, 1363–1378, doi:10.5194/acp-18-1363-2018, 2018a.
- 855 Sun, W., Maseyk, K., Lett, C. and Seibt, U.: Stomatal control of leaf fluxes of carbonyl sulfide and CO₂ in a *Typha* freshwater marsh, *Biogeosciences*, 15, 3277–3291, doi:10.5194/bg-15-3277-2018, 2018b.
- Suntharalingam, P., Kettle, A. J., Montzka, S. M. and Jacob, D. J.: Global 3-D model analysis of the seasonal cycle of atmospheric carbonyl sulfide: Implications for terrestrial vegetation uptake, *Geophys. Res. Lett.*, 35(19), L19801, doi:10.1029/2008GL034332, 2008.



- 860 Wang, Y., Deutscher, N. M., Palm, M., Warneke, T., Notholt, J., Baker, I., Berry, J., Suntharalingam, P., Jones, N., Mahieu, E., Lejeune, B., Hannigan, J., Conway, S., Mendonca, J., Strong, K., Elliott Campbell, J., Wolf, A. and Kremser, S.: Towards understanding the variability in biospheric CO₂ fluxes: Using FTIR spectrometry and a chemical transport model to investigate the sources and sinks of carbonyl sulfide and its link to CO₂, *Atmos. Chem. Phys.*, 16(4), 2123–2138, doi:10.5194/acp-16-2123-2016, 2016.
- 865 Wehr, R., Commane, R., Munger, J. W., McManus, J. B., Nelson, D. D., Zahniser, M. S., Saleska, S. R. and Wofsy, S. C.: Dynamics of canopy stomatal conductance, transpiration, and evaporation in a temperate deciduous forest, validated by carbonyl sulfide uptake, *Biogeosciences*, 14(2), 389–401, doi:10.5194/bg-14-389-2017, 2017.
- Weiner, T., Gross, A., Moreno, G., Migliavacca, M., Schruppf, M., Reichstein, M., Hilman, B., Carrara, A. and Angert, A.: Following the Turnover of Soil Bioavailable Phosphate in Mediterranean Savanna by Oxygen Stable Isotopes, *J. Geophys. Res. Biogeosciences*, 123(6), 1850–1862, doi:10.1029/2017JG004086, 2018.
- 870 Whelan, M. E. and Rhew, R. C.: Carbonyl sulfide produced by abiotic thermal and photodegradation of soil organic matter from wheat field substrate, *J. Geophys. Res.-Biogeo.*, 120(1), 54–62, doi:10.1002/2014JG002661, 2015.
- Whelan, M. E., Hilton, T. W., Berry, J. A., Berkelhammer, M., Desai, A. R. and Campbell, J. E.: Carbonyl sulfide exchange in soils for better estimates of ecosystem carbon uptake, *Atmos. Chem. Phys.*, 16(6), 3711–3726, doi:10.5194/acp-16-3711-2016, 2016.
- 875 Whelan, M. E., Lennartz, S. T., Gimeno, T. E., Wehr, R., Wohlfahrt, G., Wang, Y., Kooijmans, L. M. J., Hilton, T. W., Belviso, S., Peylin, P., Commane, R., Sun, W., Chen, H., Kuai, L., Mammarella, I., Maseyk, K., Berkelhammer, M., Li, K.-., Yakir, D., Zumkehr, A., Katayama, Y., Ogée, J., Spielmann, F. M., Kitz, F., Rastogi, B., Kesselmeier, J., Marshall, J., Erkkilä, K.-., Wingate, L., Meredith, L. K., He, W., Bunk, R., Launois, T., Vesala, T., Schmidt, J. A., Fichot, C. G., Seibt, U., Saleska, S., Saltzman, E. S., Montzka, S. A., Berry, J. A. and Campbell, J. E.: Reviews and Syntheses: Carbonyl Sulfide as a Multi-scale Tracer for Carbon and Water Cycles., *Biogeosciences*, 15, 3625–3657, doi:10.5194/bg-15-3625-2018, 2018.
- 880 Wohlfahrt, G.: Modelling Fluxes and Concentrations of CO₂, H₂O and Sensible Heat Within and Above a Mountain Meadow Canopy: A Comparison of Three Lagrangian Models and Three Parameterisation Options for the Lagrangian Time Scale, *Boundary-Layer Meteorol.*, 113(1), 43–80, doi:10.1023/B:BOUN.0000037326.40490.1f, 2004.
- 885 Wohlfahrt, G., Gerdel, K., Migliavacca, M., Rotenberg, E., Tatarinov, F., Müller, J., Hammerle, A., Julitta, T., Spielmann, F. M. and Yakir, D.: Sun-induced fluorescence and gross primary productivity during a heat wave, *Sci. Rep.*, 8(1), 14169, doi:10.1038/s41598-018-32602-z, 2018.
- Yang, F., Qubaja, R., Tatarinov, F., Rotenberg, E. and Yakir, D.: Assessing canopy performance using carbonyl sulfide measurements, *Glob. Chang. Biol.*, 24(8), 3486–3498, doi:10.1111/gcb.14145, 2018.
- 890 Yi, Z., Wang, X., Sheng, G., Zhang, D., Zhou, G. and Fu, J.: Soil uptake of carbonyl sulfide in subtropical forests with different successional stages in south China, *J. Geophys. Res. Atmos.*, 112(D8), doi:10.1029/2006JD008048, 2007.